SEMIANALYTICAL CALCULATION OF THE 0^{++} GLUEBALL MASS IN SU(2) GAUGE THEORY

Thesis by

Adam Kolawa

In Partial Fulfillment of the Requirements

for the Degree of

Doctor of Philosophy

California Institute of Technology

Pasadena, California

1986

(Submitted March 17, 1986)

Acknowledgements

I would like to thank my physics advisor and friend, Wojtek Furmanski, for the good advice and help he has given me. I thank him for generously sharing his knowledge of physics with me.

I would also like to thank my academic advisor, Geoffrey Fox, for his encouragement, guidance and generous support. I thank him too, for introducing me to the fascinating field of parallel computing.

Thank You.

Abstract

An attempt is made to derive and to solve the Schrodinger equation in the low energy region (vacuum, first excitation etc.) of the lattice. The complete orthonormal basis in the physical Hilbert space is constructed by classifying independent solutions of the Gauss' law. Loops of electric flux are chosen as elementary variables. The loop space Hamiltonian is derived, an ansatz is made for the low–energy wave functionals and the Schrodinger equation is solved in the (truncated) loop basis.

The resulting physical picture for the Yang–Mills vacuum in the cross–over region is that of, still quite dilute, gas of fluctuating loops. The glueball in this formalism looks like a local inhomogeneity in the loop distribution. A definite candidate for the confining force emerges: the repulsive non–Abelian loop–loop interaction (rather weak but persistent) generates an effective external field ("external pressure") prohibiting unbounded loop size fluctuations. The negative sign (repulsion) is universal for all compact groups.

Contents

Introduction

The basic aim of High Energy Physics is to understand what the fundamental constituents of matter are and how they interact with each other. Among the well–known strong, electromagnetic, weak and gravitational interactions, the latter three have been rather well understood, at least in a certain limit (lowest order, classical etc.). But the solution of the strong interaction problem still eludes the physicists. The only realistic candidate field theory of strong interactions that is both renormalizable and consistent with the known symmetry properties of the hadrons is Quantum Chromodynamics (QCD). It is unambiguously defined and is capable of describing qualitatively the experimental data. However, even more than a decade after it was first proposed, we are still far from the full quantitative understanding of the theory.

QCD is a gauge theory describing the interaction between spin $\frac{1}{2}$ quarks and massless vector gluons. The difficulty in constructing reliable computational methods stems from the fact that though the interaction is weak at short distances, a property known as asymptotic freedom, it grows strong at long distances. The expected physical spectrum should consist not of free quarks and gluons, but only of color singlet bound states – candidates for hadrons. In high energy experiments, at large enough momenta where the coupling is weak enough to make the quark–gluon language adequate, one can use the standard renormalization group improved perturbation theory to calculate the predictions of QCD, and these do agree reasonably well with the experimental results. But to make sure that the theory is correct as a whole, one has to solve the problem of how quarks and gluons turn into hadrons as the coupling becomes stronger at lower momentum scales. It is an intriguing and unsolved problem, as to whether or not the theory constructed locally has the right global non–perturbative properties. To analyze this problem, quantitative non–perturbative methods are needed: methods, where the approximations can be controlled, and where there

exists the possibility of improving the calculation by increasing the computational effort.

The existing non–perturbative methods like the large N expansion, the mean field technique and instanton calculations provide some qualitative understanding of non–perturbative phenomena, but they do not provide results which can be directly compared with Particle Data. On the other hand, Monte–Carlo techniques on the lattice, although numerically successful, are still unable to give good insight into the dynamics of the gauge fields, at least with the current computing power.

This work is an attempt to compromise and to interpolate between the qualitative and quantitative techniques, and to develop a semianalytic approach to the quantum field theory formulated on the space–time lattice.

Even in the absence of quarks, QCD is a highly non–linear and complicated field theory of gluons interacting with each other. Phenomena such as confinement are expected to be present in a simpler theory than QCD – the pure Yang–Mills field theory. The study of the pure Yang–Mills gauge theory is a natural first step towards the understanding of the non–perturbative aspects of QCD. In this work the Yang–Mills theory is used as an example on which the semianalytic technique is developed. The method has been described in [13].

Our strategy in the semianalytic approach is to reduce first the gauge system to physical variables – this can be done analytically to a large extent – and then to solve numerically the reduced "physical" problem. Proceeding this way, one can hope to get both numbers and intuitive understanding.

The natural route to the physical degrees of freedom is via the Hamiltonian formalism in the temporal gauge. To get rid of the residual time–independent gauge symmetry, one has to extract the physical Hilbert subspace, which is accomplished by imposing and solving Gauss' law.

As the first step in this program, we have classified the independent solutions of Gauss' law, and we have constructed the complete orthonormal basis of states in the physical Hilbert space. Next, an attempt has been made to solve the Schrodinger equation for the 0^{++} glueball mass, using two different computational methods. The first method, simpler, more computer–oriented, is based on the idea borrowed from the theory of the Mathieu equation in non–relativistic quantum mechanics. This method has numerical difficulties and problems with stability, which are caused by various infrared infinities (volume effects). Using the Mathieu–like method as a guide, we tried next to construct a more realistic computational scheme, with the volume effects factored out by means of the appropriate ansatz for the wave functionals (cluster expansion in the loop space). The latter method is used to calculate the 0^{++} glueball mass in $SU(2)$ gauge theory.

Chapter 1 contains a general overview of the Yang–Mills theory and a brief discussion of the relevant non–perturbative methods. In Chapter 2 the description of Gauss' Law is presented and the complete orthonormal basis is constructed. Chapter 3 presents an attempt to solve the Schrodinger equation and to calculate the 0^{++} glueball mass in the Yang–Mills theory, using the first computational technique. This chapter also describes the sequential and concurrent computer program to produce states in the Hilbert space. Chapter 4 contains the description of the second method, presenting both a general formalism as well as an intuitive explanation of factorization. The results of calculation of the 0^{++} glueball mass in the Yang–Mills theory are presented in the last part of chapter 4. Chapter 5 contains conclusions.

1. Introduction to Lattice Gauge Theories.

1.1 Yang–Mills Theory.

Yang–Mills theory is defined on the classical level by the following lagrangian:

$$L = \frac{1}{2} tr\, F_{\mu\nu} F^{\mu\nu} , \tag{1.1}$$

where

$$D_\mu = \partial_\mu - igA_\mu , \tag{1.2}$$

$$A_\mu = A_\mu^a T^a , \tag{1.3}$$

$$F_{\mu\nu} = \partial_\mu A_\nu - \partial_\nu A_\mu - ig[A_\mu, A_\nu] . \tag{1.4}$$

A_μ^ν is the vector gauge field. T^a are the SU(2) gauge group generators, conventionally normalized to the delta function :

$$tr\, T^a T^b = \frac{1}{2}\delta^{ab} . \tag{1.5}$$

The theory is invariant under local SU(2) gauge transformation:

$$A_\mu(x) \to \Omega(x) A_\mu(x) \Omega^{-1}(x) + \frac{1}{ig}(\partial_\mu \Omega(x))\Omega^{-1}(x) , \tag{1.6}$$

where $\Omega(x)$ is SU(2) matrix.

It is expected that only the singlet sector of the theory is physically relevant, i.e., that all physical quantities like spectrum, scattering amplitudes etc. are gauge–invariant, whereas all higher representations of the gauge group have infinite energies and they are absent on the list of observables (the phenomenon conventionally referred to as "confinement" of the gauge degrees of freedom).

1.2 Quantization of the Classical Field Theory.

Once the theory is formulated on the classical level, it can be quantized by one of the standard methods. The most elegant way of quantization is through the Feynman Path Integral formalism.

Let $S[\phi]$ be the action of a classical field theory :

$$S[\phi] = \int dx L(\phi(x)) , \tag{1.7}$$

where $L(\phi(x))$ is the lagrangian of the theory and $\phi(x)$ represents all the fields in this theory. The integration is carried over the whole space–time.

The quantum amplitudes are calculated by averaging the classical expressions over all field configurations, weighted with the exponential of the action. E.g., in units $h=c=1$, the vacuum–to–vacuum transition ("generating functional") takes the form:

$$Z = \int d[\phi] e^{iS[\phi]} , \tag{1.8}$$

and the quantum vacuum expectation value of an operator $O[\phi]$ is given by :

$$< O[\phi] > = \frac{\int d[\phi]\, O[\phi] e^{iS[\phi]}}{\int d[\phi]\, e^{iS[\phi]}} . \tag{1.9}$$

The complex measure in the formulas (1.8–1.9) oscillates very rapidly around the classical value of the action. There is a large amount of cancellation between the interfering phases, and most of the contribution comes from the integrals with stationary phases. This is more easily understood after performing the Wick rotation to imaginary time $t \to i\tau$, which defines the theory in the Euclidean space. The complex phase is transformed into an exponentially damping factor, and the resulting Euclidean field theory becomes equivalent to some well–defined problem from statistical mechanics. After the Wick rotation the formula (1.9) takes the form :

$$< O[\phi] > = \frac{\int d[\phi]\, O[\phi] e^{-S[\phi]}}{\int d[\phi]\, e^{-S[\phi]}} . \qquad (1.10)$$

1.3 Lattice as an Ultraviolet Regulator.

The Feynman path integral as defined in Eq. (1.8) has ultraviolet divergences which must be regulated. One of the methods, particularly useful in the low–energy region is to replace the continuous Euclidean space by a discrete lattice. Consider the regular hyper–cubic lattice. The lattice unit is denoted by "a", the lattice point by $n_\mu=(n_1,n_2,n_3,n_4)$. The Fourier transform of a function $f(n)$ defined on the lattice is given as :

$$\tilde{f}(p) = a^4 \sum_n e^{ipna} f(n) . \qquad (1.11)$$

The function $\tilde{f}(p)$ is periodic over $p^\mu = 2\pi/a$; therefore, the momentum values can be constrained within the first Brillouin zone :

$$-\pi/a \leqq p_\mu \leqq \pi/a . \qquad (1.12)$$

Thus, the lattice provides for a cutoff in the momentum space.

The lattice regularization destroys the Lorentz invariance of the theory which, according to common belief, is expected to be restored dynamically in the continuum limit $a \to 0$ [3].

Given the continuum lagrangian, there is a natural way to define the field theory on the lattice : scalar fields are defined on points, vector fields, on links of the lattice, and derivatives are replaced by finite differences :

$$\partial_\mu f(x) \to \Delta_\mu f(n) = 1/a(f(n+\mu) - f(n)) , \qquad (1.13)$$

where μ is the unit vector along the μ direction. However, this definition does not preserve the gauge symmetry of the theory. The local gauge invariance is an intrinsic part of the dynamics, and hence we want to retain it while formulating

the theory on the lattice. For this reason, it is convenient to work with the manifestly gauge–invariant quantity – connection, i.e., the exponential of the path–ordered line integral of the gauge field $A_\mu(x)$,

$$K(1,2) = exp\,[\, ig \int_1^2 dx^\mu A_\mu(x)\,]. \tag{1.14}$$

As shown by Wilson et al. [1], the gauge invariant lattice theory can be formulated in the natural way in terms of these connections between adjacent lattice sites, $U_\mu(n)$,

$$U_\mu(n) = e^{-igaA_\mu(n)}\,, \tag{1.15}$$

rather than directly in terms of the gauge fields $A_\mu(x)$. Here A_μ are the group matrices in the adjoint representation, and the variables $U_\mu(n)$ live on links going from the site n to the site $n+\mu$. The gauge invariant action is defined in terms of closed loops of link matrices. The simplest choice is,

$$S[U] = \beta \sum_{plaqs} S_{plaq}\,, \tag{1.16}$$

$$S_{plaq} = \frac{1}{2N} tr(U_\mu(n)U_\nu(n+\mu)U_\mu^{-1}(n+\nu)U_\nu^{-1}(n) + h.c.)\,. \tag{1.17}$$

Here g is the coupling constant. The sum in Eq. (1.16) is over all the plaquettes and the trace in Eq. (1.17) is taken around a single plaquette.

The action defined in Eq. (1.16) is explicitly invariant under the local gauge transformation by a unitary matrix V_n in every lattice point :

$$U_\mu(n) \to V_n U_\mu(n) V_{n+\mu}^+\,. \tag{1.18}$$

The action in Eq. (1.16) respects maximally the symmetries of the lattice: it is invariant under $\pi/4$ rotations and lattice translations. It is also invariant under parity transformation and charge conjugation, but it breaks, as was mentioned before, the Lorentz symmetry.

The action (1.16) expanded in terms of the lattice constant " a " should reproduce the continuum action of formula (1.1). This leads to the following relation between β and g :

$$\beta = 2N/g^2 . \tag{1.19}$$

With the above definitions the Feynman path integral in Eq. (1.8) takes the form :

$$Z = \int \prod_{n,\mu} dU_\mu(n) e^{-\beta S[U]} . \tag{1.20}$$

1.4 Continuum Limit of the Lattice Gauge Theory.

The pure gauge theory has no dimensional parameters but the lattice spacing "a". The correct dimensions of all physical quantities calculated in such a theory must be constructed out of powers of "a". For instance, the physical mass m_{ph}, the mass calculated on the lattice $m_{lattice}$ and the lattice spacing "a" are related through the following formula:

$$m_{ph} = \frac{m_{lattice}}{a} . \tag{1.21}$$

When the theory approaches the continuum limit $a \to 0$, $m_{lattice}$ must tend to 0 in order to keep the physical mass constant. It is known from statistical physics that the inverse of the correlation length ξ is equal to the value of the mass calculated on the lattice. Thus, the relation between the physical mass and the correlation length is the following:

$$m_{ph} = \frac{1}{\xi\, a} . \tag{1.22}$$

The formula (1.22) shows another important feature of the lattice gauge theory. When the theory is close to the continuum limit, the correlation length

goes to ∞. Thus, the lattice system approaches the second–order phase transition. The hope is (and there are some insights from the Monte–Carlo calculations [6,7]) that Yang–Mills gauge theory on the lattice has only one phase transition with $a \to 0$, $g \to 0$. At this point the lattice theory is the continuous Yang–Mills field theory. In the vicinity of the critical point, the coupling constant and the lattice spacing "a" should obey the general scaling equation from perturbative Yang–Mills theory [16] :

$$\beta(g) = a\frac{d}{da}g(a) . \tag{1.23}$$

In general, the $\beta(g)$ function depends on the renormalization scheme, but the first two terms of its expansion in terms of g are scheme–independent and are :

$$\beta(g) = \beta_0 g^3 + \beta_1 g^5 + \cdots , \tag{1.24}$$

where

$$\beta_0 = \frac{1}{16\pi^2}\ \frac{11N}{3} , \tag{1.25}$$

$$\beta_1 = (\frac{1}{16\pi^2})^2\ \frac{34N^2}{3} , \tag{1.26}$$

and N is the number of colors.

The last three equations allows us to solve Eq. (1.23) for " a ":

$$a = \frac{1}{\Lambda_0}(g^2\beta_0)^{\beta_1/(2\beta_0^2)}\, exp(-1/(2\beta_0 g^2)) , \tag{1.27}$$

where

$$\Lambda_0 = \frac{\Lambda_R}{57.5} ,\ \Lambda_R \sim 200MeV . \tag{1.28}$$

The Λ_0 is the integration constant [4,5] and Λ_R for $SU(3)$ theory is determined

from experiments.

From Eqs. (1.22) and (1.27) we can derive the correlation length as a function of the coupling constant :

$$\xi = \frac{\Lambda_0}{m_{ph}} (g^2\beta_0)^{-\beta_1/(2\beta_0^2)} exp(1/(2\beta_0 g^2)) , \tag{1.29}$$

where m_{ph} is the physical mass.

1.5 Calculational Methods in the Lattice Gauge Theories.

Most of the calculational methods in the lattice gauge theories come from statistical physics. The essential elements of the Monte–Carlo simulations, mean field techniques and strong coupling expansion, will be discussed briefly.

a) Monte–Carlo simulations.

At present, Monte–Carlo simulation is the most powerful technique for the quantitative study of the lattice gauge theories.

For any operator O its vacuum expectation value is defined as:

$$< O > = \frac{1}{Z} \int d[\phi] O(\phi) e^{-S[\phi]} . \tag{1.30}$$

On a finite lattice this is a well–defined problem (finite–dimensional integral) but, even on a relatively small lattice, like 10^4 for SU(2) gauge theory, there are 120,000 independent variables to be integrated over. This huge multidimensional integral can be calculated numerically by summing over randomly generated field configurations. But, due to the Boltzman factor e^{-S}, the integrand changes very rapidly, and with naive (flat distribution) random sampling one would generate most of the time–irrelevant field configurations. The important configurations should be generated with the probability distribution [17]:

$$P([\phi]) \sim e^{-S[\phi]} . \tag{1.31}$$

With this "importance sampling" the integral (1.30) takes the form:

$$< O > = \frac{1}{M} \sum_{\phi_i} O[\phi_i] , \tag{1.32}$$

where M is the number of generated field configurations. The statistical errors of these calculations decrease like $\frac{1}{\sqrt{M}}$ (modulo volume effects).

In Monte Carlo method some quantities such as the string tension or the $\overline{q}q$ potential can be calculated relatively easily.

The string tension is defined as the coefficient K in the "area law" :

$$< W > \sim e^{-a^2 J*I*K} , \tag{1.33}$$

where W is a rectangular Wilson loop with the edges of size, respectively, J ,I. When the theory approaches the continuum limit, the string tension should scale like $1/a^2$. Figures 1 and 2 show results of the Monte Carlo calculations of the string tension for the SU(2) and SU(3) gauge theory [6,7]. These pictures were intentionally chosen to present calculations on relatively small lattices , where the correlation length in the "scaling window" must be of order of few lattice units. In our approach we consider the rapid onset of scaling in the Monte–Carlo calculations as a kind of " experimental data" about the low–energy behavior of the lattice Yang–Mills theory, and we try to build a more analytical calculation scheme, based on this observation.

b) The mean–field technique.

The mean–field method is a well–known procedure in statistical physics [18]. It is a quick, easy method to obtain some information about the system, and in many cases it works well in predicting the existence and location of phase transitions.

In the mean–field analysis one concentrates on a single link in the partition function. The effect of all other links is replaced by a mean–field value Λ, which

is taken to be proportional to the unit matrix. In this approximation the action is reduced to:

$$S[\phi] = \sum_{plaq} S_{plaq} \rightarrow 2*(d-1)*\Lambda^3(trU_{\mu\nu}+h.c.) \tag{1.34}$$

$$+ \textit{terms independent of } U_{\mu\nu} ,$$

where $U_{\mu\nu}$ is the SU(N) matrix on the link under consideration and d is the number of the space time–dimensions. The consistency requirement is :

$$\frac{1}{N}<\frac{1}{2}(trU_{\mu\nu} + h.c.)> = \Lambda . \tag{1.35}$$

Solution of this equation allows us to determine the phase transitions of the theory under consideration. For simple spin models, the predictions of Eq. (1.35) agree quite well with the known phase transition points. For SU(2) and SU(3) gauge theories, where no deconfining phase transition is expected to occur, it is hoped (and there are indications for that) that the phase transition, predicted by the lowest approximation, disappears after including systematically higher–order effects.

The mean–field method has not yet become a new quantitative method in lattice gauge theories, although it provides a very crude overall picture of the cross–over region (strong–coupling → weak coupling transition region).

c) The high temperature expansion.

The high temperature expansion is a systematic expansion in $1/g^2$, starting from the exact confining solution at $g = \infty$. The idea is to derive a reasonably long series for the physical quantity in question and then to extrapolate this power series towards the continuum point $g = 0$ [19,20].

There are two equivalent ways to do the high temperature expansion. The first is by expanding the path integral in Eq. (1.20) in terms of $1/g^2$. The second is the standard perturbation theory in the Hamiltonian formalism. This type of

expansion will be discussed in the following chapters.

The high temperature expansion in the Lagrange formalism is slightly aside from the main stream of this work, and it will be discussed only briefly on an example of the calculation of the Wilson loop operator $<W(C)>$.

The Boltzman factor in Eq. (1.30) is a class function on the group SU(N). Thus, it can be expanded in a character series:

$$e^{\beta(trU_p + h.c.)} = \sum_r d_r \beta_r(\beta)\, \chi_r(U_p)\,, \tag{1.36}$$

where d_r denotes the dimension of the representation r. The orthogonality relation for characters allows us to determine the constants β_r :

$$\int dU \chi_r(SU)\bar{\chi}_s(U) = \frac{\delta_{rs}}{d_r}\chi_r(S)\,. \tag{1.37}$$

The Wilson loop $<W(C)>$ is the trace of the product of group matrices U along the curve C. The lowest order of the expansion is given by the configuration with the minimal area of the Wilson loop covered by plaquettes. Thus, the Wilson loop in the lowest order will be proportional to some (g dependent) constant raised to the power of the area of the loop :

$$<W(C)> = C^{\,-area/a^2}\,. \tag{1.38}$$

This shows that to lowest order, the high temperature expansion gives a confinement phase of QCD [8]. The higher orders of the expansion are obtained by building more and more complicated surfaces over the Wilson loop.

2. Description of the Method.

2.1 General Idea.

The goal of this work is to develop a semianalytic method for low–energy calculations (vacuum, mass gap) in SU(2) gauge theory and to apply it. Semi–analytic technique requires keeping track of a large number of variables. For this reason, it is essential to reduce the number of fields in the theory to a minimal possible set. It is also convenient to have variables that are mostly linearly independent.

The lattice gauge theory, as presented in Chapter 1 (Section 2), has many degrees of freedom that are redundant, and they may be eliminated from the theory. The first step on the way to reducing the number of variables is to pass from the Lagrangian formalism to the Hamiltonian formulation and to get rid of the time dependence. The transition to the Hamiltonian language is realized by fixing the gauge $A_0=0$ (temporal gauge). The theory still has the residual gauge freedom in 3 spatial dimensions; i.e., it is invariant under the time–independent gauge transformations . This freedom is removed by restricting the Hilbert space to the "physical sector", given by solutions of Gauss' Law.

It is very difficult to solve Gauss' Law in the basis of eigenstates of the vector potential $|A>$. It is more natural to use for this purpose the electric field basis $|E>$, where the requirement of the gauge invariance imposes simply the continuity condition of the flux lines. The $|E>$ basis also has another nice feature: for large coupling constant g , the gauge theory is in the electric confinement phase and electric fluxes are stable. On the other hand, the vector potential A fluctuates very rapidly in this region. When $g\to 0$, the electric flux starts to fluctuate and more and more degrees of freedom are activated in the $|E>$ basis. The hope, supported by the Monte–Carlo calculations (Chapter 1), is that the correlation length is still reasonably small in the region of g where the scaling behavior sets on. This leads to the expectation that fluctuations of the electric

flux are moderate in the "scaling window" and $|E>$ can still be efficiently used as a basis for calculations.

In the electric flux basis it is possible to choose variables, closed loops of electric flux, such that they automatically obey Gauss' Law.

The structure of this chapter is the following:

Section 2 :Derivation of the Hamiltonian for the SU(2) gauge theory in E basis.

Section 3: Solution of Gauss' Law.

Section 4: Possible choices of basis variables.

2.2 Derivation of Hamiltonian for the SU(2) Gauge Theory.

Derivation of the Hamiltonian for SU(N) gauge theory was first done by Kogut and Susskind by using the standard prescription for canonical quantization [2]. We present here another method based on the transfer matrix formalism. Most of this section is valid for any SU(N) gauge theory. Only in the last part of the derivation we use some special features of SU(2).

The starting point is the action for the SU(2) gauge theory in Eq. (1.16):

$$S = -\sum_{palqs}\frac{\beta}{2N}(Tr(UUU^{+}U^{+})+h.c.), \tag{2.1}$$

where

$$U = e^{-iga A^{\mu}}. \tag{2.2}$$

In the gauge A_0=0 all matrices in the time direction are one (U_0=1). Thus, the action in Eq. (2.1) can be divided into two parts:

$$S = -\sum_{plaqs_{space}}\frac{\beta}{2N}(Tr(UUU^{+}U^{+})+h.c.)-\sum_{plaqs_{time}}\frac{\beta_0}{2N}(Tr(UU^{+})+h.c.)\,. \tag{2.3}$$

Summation in the first term goes over all spatial plaquettes (these which do not have any link pointing in the time direction). The second sum goes over all

plaquettes which have a link pointing in the time direction. In general, β and β_0 (coupling in the time direction) can be different. They are related to the original coupling constant g, spatial lattice spacing a , and time lattice spacing a_0 through the following relations :

$$\beta = \frac{a_0 2N}{ag^2} , \tag{2.4}$$

$$\beta_0 = \frac{a\,2N}{a_0 g^2} .$$

To find the Hamiltonian, one needs to define a Hilbert space on which the Hamiltonian acts, and to derive an explicit form of the Hamiltonian in this space. The Hamiltonian is an operator that transforms a system in time between two infinitesimal time slices. The corresponding discrete operator, which transforms in the time direction between two adjacent configurations on the lattice, is the transfer matrix, often used in statistical physics. The transfer matrix is defined through the equation:

$$Z = \int dU\, e^{-S} = Tr T^M , \tag{2.5}$$

where Z is the vacuum–to–vacuum transition amplitude in Eq.(1.8), M is the size of the lattice in the time direction. In the limit $a_0 \to 0$ the transfer matrix is related to the Hamiltonian H through the infinitesimal relation:

$$T = e^{-a_0 H} = 1 - a_0 H . \tag{2.6}$$

The space of states for the Hamiltonian is constructed as a tensor product of single link states $|g, n\mu\rangle$ parameterized by group elements $g \in SU(N)$ on every link, μ , the direction of the link, and $n = (n_0, n_x, n_y, n_z)$, the vertex from which the link comes out. In this space, one can define two useful operators: the representation operator $G^r_{\alpha\beta}$, and the group multiplication operator D. The representation operator, acting on the state $|g, n\mu\rangle$ multiplies it by the

representation matrix in the representation r :

$$G^r_{\alpha\beta}\,|g,n\mu> = R^r_{\alpha\beta}(g)\,|g,n\mu> . \tag{2.7}$$

In particular, for $r=f=$ the fundamental representation, we have $R^f_{\alpha\beta}(g)=U_{\alpha\beta}(g)$. The group operator, D, realizes shifts in the group space:

$$D(h)\,|g,n\mu> = |hg,n\mu> . \tag{2.8}$$

The explicit form of the transfer matrix will be derived from Eq. (2.5) by inserting between every pair of adjacent T operators the full spectrum of states in the three-dimensional lattice ($|g>$ represents the tensor product of states in 3D space) :

$$Z = Tr(T...T) = \int dg'dg_1 \cdots <g'\,|T\,|g_1> \cdots <g_{N-1}|\,T\,|g'> . \tag{2.9}$$

The above relation together with (2.3) implies that :

$$<g_{n_0}|\,T\,|g_{n_0+1}> = e^{-\frac{1}{2}S_{h\,n_0}-S_0(g_{n_0},g_{n_0+1})-\frac{1}{2}S_{h\,n_0+1}} , \tag{2.10}$$

where $S_{h\,n_0}$ is the action in 3-D space (fixed time slice), and $S_0(g_{n_0},g_{n_0+1})$ is the single bit of action in the time direction. Equation (2.10) suggests that the operator T should be constructed out of two different operators. The first one, acting on state $|g_{n_0}>$ ($|g_{n_0}+1>$), should give the part of the action $e^{-\frac{1}{2}S_{h\,n_0}}$ ($e^{-\frac{1}{2}S_{h\,n_0+1}}$). This operator acts only on the space links. It can be constructed by replacing all U by G in the first term of Eq. (2.3) . The second operator, which should produce action in the time direction ($e^{-S_0(g_{n_0},g_{n_0}+1)}$), acts between two subsequent 3D configurations, shifted by one lattice unit in time. It can not be constructed in this simple way. The term $e^{-S_0(g_{n_0},g_{n_0}+1)}$ is a class function on the group; thus, it can be expanded into the character series:

$$e^{-S_0(g_{n_0},g_{n_0+1})} = \sum_{n=n_x,n_y,n_z}\sum_r e^{\beta^*_r}\chi^r(g^{-1}(n_0)g(n_0+1)) . \tag{2.11}$$

The β_r^* is a numerical coefficient and is calculated in Appendix A.

To proceed further, one defines the projection operator Λ:

$$\Lambda^r = d_r \int dg\, \chi^r(g^{-1}) D(g)\,, \tag{2.12}$$

where d_r is the dimension of the representation. It is easy to see that the matrix element of the operator Λ^r between two states $|g_{n_0}$, $|g_{n_0+1}$ is :

$$<g_{n_0}|\Lambda^r|g_{n_0+1}> = d_r \chi_r(g^{-1}(n_0) g(n_0+1)). \tag{2.12a}$$

Projective properties of Λ^r together with Eqs. (2.11) and (2.12a) lead to the following form for the e^{-S} :

$$e^{-S_0(g_{n_0}, g_{n_0+1})} = <g_{n_0}| e^{-\sum_r \beta_r^* \Lambda_r} |g_{n_0+1}>\,. \tag{2.13}$$

Thus, the final operator form of the T matrix can be written :

$$T = e^{-\frac{1}{2}V} e^{-\Lambda} e^{-\frac{1}{2}V}\,, \tag{2.14}$$

where V represents S_h with U matrices replaced by G operators, and

$$\Lambda = -\sum_r \beta_r^* \Lambda_r\,. \tag{2.15}$$

As already discussed, the basis $|g, n\mu>$ – the vector potential basis (denoted by $|A>$ in Section 2.1) – is not very convenient to solve Gauss' Law, and it is better to Fourier–transform it to an electric field basis $|r, \alpha\beta, n\mu>$(denoted by $|E>$ in Section 2.1) through the following transformation :

$$|r, \alpha\beta, n\mu> = \sqrt{d_r} \int dg\; R^r_{\alpha\beta}(g^{-1})\, |g, n\mu>\,. \tag{2.16}$$

In this basis operator Λ is the Casimir operator for the $SU(N)$ group, and operator V is the rising/lowering operator in the representation space.

The final step to get the Hamiltonian is to take $a \to 0$ limit in Eq. (2.14). The result of this operation for SU(2) gauge theory is the following :

$$T = e^{-\frac{a_0}{a}(-\frac{2}{\beta}\sum_l r(r+1) + \frac{\beta}{2}\sum_p S_p)}, \tag{2.17}$$

where S_p is the action for a given time slice. The first/second sum in the Eq. (2.17) runs over all links/plaquettes. The Hamiltonian can be extracted from the Eq. (2.17):

$$H = -\frac{2}{\beta}\sum_l r(r+1) + \frac{\beta}{2}\sum_p S_p \,. \tag{2.18}$$

2.3 Solution of Gauss' Law.

In the electric flux basis every state on the lattice $|\Psi>$ is a tensor product of $|r,\alpha\beta,n\mu>$[1] on each link:

$$|\Psi> = \sum_{l\alpha\beta} F^{l_1 l_2 \cdots}_{\alpha_1\beta_1,\alpha_2\beta_2,\cdots} \; |l_1,\alpha_1\beta_1,n_1\mu_1> |l_2,\alpha_2\beta_2,n_2\mu_2> \cdots$$

where the product is over all sites and the sum is over all indices $l\alpha\beta$. The functional F is yet unknown. Gauss' Law in the operator language demands that a state on the lattice must be invariant under local gauge transformation :

$$(\prod_n \Omega(n,a))|\Psi> = |\Psi> \,, \tag{2.19}$$

where $|\Psi>$ represents a global state on the lattice and $\Omega(n,a)$ is the gauge symmetry operator acting at the vertex n with the group element a. In the $|r,\alpha\beta>$ basis the operator $\Omega(n,a)$ acts by multiplying each link outgoing from vertex n by the representation matrix $R^r_{\mu\nu}(a)$. Suppose first, for simplicity, that each vertex has only three outgoing links instead of six . Let $V_{\alpha\beta\gamma}(n)$ be the function

[1] From now on we will use the shorthand notation $|r,\alpha\beta>$ to label the states in the $|E>$ basis.

which is used in vertex n to contract indices (V is the part of the functional F). Then the state $|\Psi>$ can be written as:

$$|\Psi> = |l,\alpha\alpha_1> |m,\beta\beta_1> |n,\gamma\gamma_1> V_{\alpha\beta\gamma}(n) \; |\Psi_{\alpha_1\beta_1\gamma_1}>. \qquad (2.20)$$

The indices $\alpha_1,\beta_1,\gamma_1$ are connected to the remaining part of the state – $|\Psi_{\alpha_1\beta_1\gamma_1}>$.

The operator $\Omega(a,n)$ acting on link variable $|l,\alpha\alpha_1>$ multiplies it by $R^l_{\alpha\alpha}(a)$, the representation matrix. The condition in Eq. (2.19) implies that the function $V_{\alpha\beta\gamma}$ in each vertex must obey the following relation :

$$\sum_{\alpha\beta\gamma} R^l_{\alpha\alpha}(a)\, R^m_{\beta\beta}(a)\, R^n_{\gamma\gamma}(a)\, V_{\alpha\beta\gamma}(n) = V_{\alpha\beta\gamma}(n)\,. \qquad (2.21)$$

The Eq. (2.21) is valid for each value of a. Thus, it can be integrated on both sides over the whole group:

$$\int da\; R^l_{\alpha\alpha}(a)\, R^{m(a)}_{\beta\beta}\, R^n_{\gamma\gamma}(a)\, V_{\alpha\beta\gamma}(n) = V_{\alpha\beta\gamma}(n)\,. \qquad (2.22)$$

Using the Clebsch–Gordon coefficients, the left–hand side can be reduced to :

$$\int da\; f^{lmk}_{\alpha\beta x} f^{lmk}_{\alpha\beta y}\, R^k_{xy}(a)\, R^n_{\gamma\gamma}(a)\, V_{\alpha\beta\gamma}(n) = V_{\alpha\beta\gamma}(n)\,. \qquad (2.23)$$

The representation matrices $R^n_{\gamma\gamma}$ are orthogonal; thus, the formula (2.22) takes the form :

$$f^{lmk}_{\alpha\beta x} f^{lmk}_{\alpha\beta y}\, \delta_{kn}\, \delta_{x\gamma}\, \delta_{y\gamma}\, V_{\alpha\beta\gamma}(n) = V_{\alpha\beta\gamma}(n)\,, \qquad (2.24)$$

and

$$f^{lmn}_{\alpha\beta\gamma}(f^{lmn}_{\alpha\beta\gamma}\, V_{\alpha\beta\gamma}(n)) = V_{\alpha\beta\gamma}(n)\,. \qquad (2.25)$$

In the last equation $f^{lmn}_{\alpha\beta\gamma} V_{\alpha\beta\gamma}(n)$ has all indices contracted and it can be regarded as a constant. Thus, the form of the function V in case of three links going out of each vertex is :

$$V_{\alpha\beta\gamma} = C\, f^{lmn}_{\alpha\beta\gamma}\,. \tag{2.26}$$

Applying the same argument at each lattice site we can reduce the whole functional F to the product of Clebsch–Gordon coefficients with the indices α,β attached to appropriate states $|r,\alpha\beta>$. In consequence, any physical state is fully specified by the representations l,m,n. The numbers l,m,n obey the triangle inequality at each vertex:

$$l+m-n\geq 0,\quad m+n-l\geq 0,\quad n+l-m\geq 0.$$

The construction in the real 3–dimensional space is very similar to the example presented above. The structure of the vertex in this case is presented in Fig. 4. Every vertex has four Clebsch–Gordon coefficients and three new variables called "r". Again all the variables should obey triangle inequality for every Clebsch–Gordon Coefficient, as pointed in the picture.

$$r_\mu + r_\nu - r_\rho \geq 0,\ \mu\neq\nu\neq\rho\,. \tag{2.27}$$

The description of the physical state is in terms of a set of variables $\{l\}$, representations in links, and supplementary variables $\{\,r\,\}$, which reside on vertices.

2.4 Possible Choices of Basis Variables.

As pointed out in the previous section, the state can be uniquely described by the set of variables $\{\,\{l\},\{r\}\,\}$. The only flaw of this parameterization is that one must keep track of the triangle inequality when the state is constructed.

There is a way to visualize global aspects of the triangle inequality constraints. One can draw a vacuum diagram combining elements from Fig. 4b, according to the following rules:

1) each black dot has three white neighbors,

2) each white dot has two whites and one black,

3) each loop contains at least four blacks.

One then draws a triangle around each dot with the edges equal to appropriate values of l and r. Since any two adjacent triangles have a matching edge, all edges match somehow, and we obtain as a result the closed trangulated surface. This surface is in the one–to–one correspondence with the set of variables l, r.

In the continuum limit $\beta \to \infty$, when all triangles fluctuate ($l, r \gg 0$), the surface can be very complicated. For small β the surface collapses to very simple structures; e.g., the temperature vacuum (all l, r are zero) corresponds to a single point, one excited plaquette – to a single edge etc.. In the intermediate β regions, $l, r = 0, 1, 2$ with rapidly decreasing amplitudes for higher excitations, the surface probably has a structure of independent bubbles of size a few lattice units.

The triangle inequality (2.27) can be resolved locally by the following change of variables:

$$r_x = f_{xy} + f_{xz}, \; r_y = f_{xy} + f_{yz}, \; r_z = f_{yz} + f_{xz}. \tag{2.28}$$

The flow variables f are now non–negative, independent integers.

Introduction of the flow variables admits a natural hydrodynamical intuition, we will use throughout this work. Imagine a vacuum diagram in Fig. 5a, defining the physical states, as built from pipes filled with quantized liquid (integer flow lines f). The pipes are connected at vertices in such a way that all three flows are possible.

By introducing the flow variables, one shifts the constraint from the vertex to the link where it is required that the flow lines continuously connect adjacent vertices. The above requirements can be easily fulfilled by introducing closed loops of electric flux. One can realize various admissible configurations of the

l,r field by injecting closed loops of unit electric flux into the network on Fig. 5a in all possible ways. The fluxes l,r are derived by counting the loop lines flowing in corresponding pipes.

Any set of variables { {r},{l} } obeying the triangle inequality can be loop–decomposed. The decomposition is not unique. In consequence, there are zero modes in the loop space, activated when loops touch or overlap. (Two simple examples of possible degeneracies are given in Fig. 12a.) The existence of these modes is a quantum effect – one cannot measure simultaneously all shape details. What can be measured depends on the convention . With our choice of the vertex (Fig. 4a), the good quantum numbers are:

a) number of flux lines going through the vertex without changing direction,

b) number of flux lines changing direction.

The flow decomposition of the vertex constraint in the way presented above looks special to the $SU(2)$ case, but is in fact a general procedure, applicable to any compact group. Actually, it is equivalent to a certain graphical convention of representing the familiar Young tableaux algorithm for decomposing tensor products. For details see [13].

2.5 Hamiltonian in the Physical Hilbert Space.

The formalism described in the previous sections is very useful in semi–analytic lattice calculations. The number of variables is reduced drastically. Originally, any state was described as the product of $|r,\alpha,\beta>$ on each link contracted in α,β with some unknown functions in neighboring vertices. Gauss' Law implies that the vertex functions are determined by the group theory so that we can effectively forget about the variables α,β . They are contracted with the Clebsch–Gordon coefficients, which in turn can be regarded as built into the structure of the lattice in every vertex. The whole calculation can be carried out without explicit reference to the Clebsch–Gordon coefficients.

We now derive the action of the Hamiltonian on a given physical state on the lattice. The procedure is presented graphically (Fig.5b–9) on example of the action of the plaquette operator V_p on some general state on the lattice. (The term Λ in the Hamiltonian is diagonal in $|r,\alpha\beta>$ basis.) To derive the formula, one starts by pulling out a plaquette (on which operator V_p acts) from the network, with all attached pipes. Fig. 5b presents a convenient planar way of drawing all pipes in such a way that no lines intersect. The plaquette operator V_p acting on links multiplies them by $G^{\frac{1}{2}}_{\alpha\beta}(g)$ contracted around the plaquette. This is marked by a dotted square in Fig.6 . Using the tensor product decomposition formula one reduces products of representation matrices on each link and one obtains the result as in Fig.6 [9] . This corresponds to the following chain of identities:

$$G^{\frac{1}{2}}_{\alpha\beta}\ |n,\mu\nu> = G^{\frac{1}{2}}_{\alpha\beta}\ \sqrt{d_{\frac{1}{2}}}\int dg\ R^{n}_{\mu\nu}(g^{-1})\,|g> =$$

$$= \sqrt{d_{\frac{1}{2}}}\int dg\ R^{n}_{\mu\nu}(g^{-1})R^{\frac{1}{2}}_{\alpha\beta}(g)\,|g> = \qquad (2.29)$$

$$= \sqrt{d_{\frac{1}{2}}}\sum_{w\sigma\rho} f^{n\frac{1}{2}w}_{\mu\alpha\sigma} f^{n\frac{1}{2}w}_{\nu\beta\rho}\int dg\ R^{w}_{\sigma\rho}(g)\,|g> = \sqrt{d_{\frac{1}{2}}}\sum_{w\sigma\rho} f^{n\frac{1}{2}w}_{\mu\alpha\sigma} f^{n\frac{1}{2}w}_{\nu\beta\rho}\,|w,\sigma\rho> .$$

The dotted lines in the picture are in the fundamental representation, whereas the fat lines indicate that the representation on a given link has been "excited", i.e., raised/lowered by one unit ($l \to l' = l \pm \frac{1}{2}$). All $2^4 = 16$ contributions are summed over. Using the orthogonality of 3j symbols, one performs further reduction as indicated in Fig.7 . The final result, displayed in Fig.8, is that, going around the plaquette, all 12 pipes are excited and all 12 vertices get one-loop corrections. The vertex loop diagram can be reduced to the bare 3j vertex times the constant (which is the Wigner symbol), given by an appropriate contraction, as in Fig.9 .

The final result is:

$$V_p \mid l,r > = \sum_{s_1 s_2} P_r^l(s_1 s_2) \mid l+s_1, r+s_2 > , \qquad (2.30)$$

where $s_1, s_2 = \pm 1/2$, raising/lowering applies to each of 12 pipes building the plaquette (hence the sum in Eq. (2.30) contains $2^{12} = 4096$ terms) and the amplitudes $P_r^l(s_1 s_2)$ are given (up to a sign) by the product of 12 Wigner symbols, one per each of 12 vertices around the plaquette. The general formula for the amplitude P_r^l is given in Appendix B.

The number of terms in Eq.(2.30) is rather depressing. In practice, however, for low loop densities only a few terms in the sum are non–zero, all others being eliminated by the triangle inequalities. It is only in the very asymptotic limit $\beta \to \infty$, with all pipes full of flux, when all 4096 terms are alive.

3.The Linear Approach.

3.1 Solution of the Schrodinger Equation.

We have shown in the previous chapter how to construct the physical Hilbert space and how the Hamiltonian acts on physical states. These are our basic tools, which facilitate the low–energy calculations in the SU(2) gauge theory. There are at least two possible choices of basis in the Hilbert space: the description with the set of the local flux variables l, r and in terms of the closed loops of electric flux. In this chapter the first method will be used.

It was also shown that the Hamiltonian consists of two parts: Λ, which is diagonal and V, given by the sum of the plaquette operators V_p raising and lowering the flux representations on links . This property of the operator V_p can be used to construct an algorithm to generate states in the physical Hilbert space. The algorithm is as follows. First, the operator V_p acts in different places on empty space (all l and r equal 0) and produces one–plaquette states. We call these states the first generation. Since all one–plaquette states are translationally or rotationally equivalent, it is enough to keep only one representative (a plaquette in some randomly chosen place on the lattice). This state will be described as $|1>$.

Next, the operator V_p acts on state $|1>$, and it produces several two plaquette states (or empty space). Again, some of these two plaquette configurations are translationally or rotationally equivalent. For every different class of states only one member is kept. This state is denoted as $|2_i>$, where i labels the equivalence classes. All two plaquette states are called the second generation (in general, all n–plaquette states are called n–th generation). Acting with the operator V_p again and again, we construct states with higher and higher numbers of plaquettes. In this way one can generate (in principle) the entire Hilbert space.

Our goal is to calculate glueball mass 0^{++} . For this reason, we can restrict the above construction to states transforming as singlets under translations and cubic rotations of the lattice.

The state is uniquely described by its generation (n), its number in this generation (i) and its physical position in space. The position in space of a state can be parameterized by an element of the symmetry group of the lattice. The mapping between the group and the positions of the state is performed in the following way:

a) the position of the representative of the class to which the state belongs is assigned to the unit element of the group,

b) the position of any other state from this class is described by that element of the group by which the representative should be transformed to coincide with the state. The above parameterization is not one–to–one. To make it unique, the position of the state in space is assigned to the element g of a coset of the rotational–translational group modulo the symmetry group of the state. Using this language the state i from the n–th generation in position g will be described as $|n_i,g>$.

The one plaquette state $|\tilde{1}>$, which is singlet under translations and rotations, is defined in the following way:

$$|\tilde{1}> = \sum_{g\in G_1} |1,g> , \tag{3.1}$$

where g is an element of the one plaquette coset. The general n–th generation i–th state invariant under rotations and translations is :

$$|\tilde{n}_i> = \sum_{g\in G_i} |n_i,g> . \tag{3.2}$$

The generic 0^{++} state $|\psi>$ can be expanded as follows:

$$|\psi> = \sum_{n,i} f_{n_i} |\tilde{n}_i> , \tag{3.3}$$

where f_{n_i} are coefficients, to be determined from the Schrodinger equation:

$$H \ |\psi> = E \ |\psi> . \tag{3.4}$$

According to Eq. (2.18) the Hamiltonian can be written as :

$$H = \Lambda + V. \tag{3.5}$$

Combining Eqs. (3.4) and (3.5) one obtains the following formula :

$$(\Lambda + V) \, |\psi> = E \, |\psi> , \tag{3.6}$$

which together with Eq. (3.3) gives :

$$(\Lambda + V) \sum_{n,i} f_{n_i} | \tilde{n}_i> = E \sum_{n,i} f_{n_i} | \tilde{n}_i> , \tag{3.7}$$

Since the operator Λ is diagonal, we have, finally:

$$\sum_{n,i} f_{n_i} \Lambda_{n_i} | \tilde{n}_i> + \sum_{n,i} f_{n_i} V \, | \tilde{n}_i> = \sum_{n,i} f_{n_i} E \ | \tilde{n}_i> . \tag{3.8}$$

The Eq. (3.8) will be used as the basis for subsequent calculations.

The equations for the wave functions f_{n_i} are constructed by multipling both sides of Eq. (3.8) by different states $| n_j>$.

The first equation is obtained by multipling Eq.(3.8) by the state of perturbative vacuum $<0|$ (empty lattice). As it was pointed out earlier, the operator V can change representations on plaquettes only by 1/2. Thus, the only states for which the scalar product $<0|V|\tilde{n}_i>$ is not zero, are states $|\tilde{1}>$. The first equation takes form :

$$\Lambda_0 f_0 + <0|V|\tilde{1}> f_1 = E \ f_0 . \tag{3.9}$$

Since Λ_0=0 (no flux), we get simply:

$$<0|V|\tilde{1}> f_1 = E \ f_0 . \tag{3.10}$$

The second equation is obtained by multipling Eq. (3.8) by state $< 1 |$. In this case only states from the second generation and state $|0>$ give a contribution to the V term in the Hamiltonian :

$$\Lambda_1 f_1 + <1|V|0> f_0 + \sum_i f_{2_i} <1|V|\tilde{2}_i> = E\, f_1 \,. \tag{3.11}$$

Following the above procedure, one gets an infinite set of linear equations for unknown functions E , f_{n_i}. This system can be made solvable by truncating it to n generations and by neglecting in the equations for the n–th generation all functions $f_{(n+1)_i}$. For example, if calculations are made only up to the third generation, the equation for the three–plaquette function f_{3_i} looks as follows :

$$\Lambda_2 f_{2_j} + <2_j|V|\tilde{1}> f_1 + \sum_i <2_j|V|\tilde{2}_i> f_{2_i} = E\, f_{2_j} \,, \tag{3.12}$$

$$\Lambda_3 f_{3_j} + \sum_i <3_j|V|\tilde{2}_i> f_{2_i} = E\, f_{3_j} \,. \tag{3.13}$$

Calculating f_{3_j} from Eq. (3.13) and inserting it into (3.12) one gets :

$$\Lambda_2 f_{2_j} - \sum_{i,k} \frac{<2_j|V|\tilde{3}_i><3_i|V|\tilde{2}_k> f_{2_k}}{\Lambda_{3_i} - E} + <2_j|V|\tilde{1}> = E f_{2_j} . \tag{3.14}$$

Taking into account Eqs. (3.10) and (3.11) with some algebra, one gets the final equation for energy :

$$E = \cfrac{<0|V|\tilde{1}><1|V|0>}{E - \Lambda_1 - \sum_l \cfrac{<1|V|\tilde{2}_l><2_l|V|\tilde{1}>}{E - \Lambda_{2_l} - \sum_k \cfrac{<2_l|V|\tilde{3}_k><3_k|V|\tilde{2}_l>}{E - \Lambda_{3_k}}}} \,. \tag{3.15}$$

The last equation can be generalized to n–th order by performing further iterations in the denominator (following Λ_{3_k}) .

The Eq. (3.15) is the n–th order algebraic equation for E . Its lowest solution gives the vacuum energy; the next lowest solution is the first excitation.

Obviously, the accuracy of the solutions depends on the number of included generations.

The last equation is very similar in structure to the Mathieu equation in non–relativistic quantum mechanics [10], so it is useful to describe the method used to solve the Mathieu equation in more detail.

3.2 The Mathieu Equation and the High Temperature Expansion.

The Mathieu equation describes a continuous Abelian spin in a homogeneous magnetic field. Tuning parameters in the appropriate way we get

$$\frac{1}{\beta}\frac{d^2}{d\phi^2}F(\phi) + 2\beta\cos\phi F(\phi) = EF(\phi)\,, \quad 0 \leqq \phi \leqq 2\pi. \tag{3.16}$$

In Fourier space

$$F(\phi) = \sum_r e^{ir\phi}F_r\,, \tag{3.17}$$

the Mathieu equation takes the form of a finite difference equation in integers:

$$\left(\frac{r^2}{\beta} + E\right)F_r = \beta(F_{r+1} + F_{r-1})\,. \tag{3.18}$$

The standard method of finding normalizable solutions of Eq.(3.18) is the following. Let us consider, e.g., the even solutions

$$F_r = F_{-r}\,. \tag{3.19}$$

Defining

$$G_r = \frac{F_{r+1}}{F_r}\,, \quad E = \beta\varepsilon\,, \quad v_r = r^2\,, \tag{3.20}$$

we get the recursive formula for the "Green's function" G

$$G_r = \frac{1}{\frac{v_{r+1}}{\beta^2} + \varepsilon - G_{r+1}}\,, \tag{3.21}$$

with the initial condition

$$2G_0 = \varepsilon \,. \tag{3.22}$$

Since the normalizability implies $G_r \to 0$ for $r \to \infty$, we are allowed to reiterate the recursion in Eq.(3.21). We get

$$\frac{1}{2}\varepsilon = \cfrac{1}{\frac{v_1}{\beta^2} + \varepsilon - \cfrac{1}{\frac{v_2}{\beta^2} + \varepsilon - \cfrac{1}{\frac{v_3}{\beta^2} + \varepsilon - \cfrac{1}{\frac{v_4}{\beta^2} + \varepsilon - \cdots}}}} \tag{3.23}$$

and similar infinite fractions for G_r's.

The last equation is very similar to Eq. (3.15). The difference is that in the Mathieu equation the coefficients are numbers and in Eq. (3.15) the coefficients are matrices. If we consider a lattice which consists of only one plaquette, then Eq. (3.15) would have the exact form of the Mathieu equation. Thus, the difference between the equations arises because of operator V acting in different places on the lattice.

Despite the differences, one may get some insight into the exact solution of the Eq. (3.4) from the solution of the Mathieu equation. The standard method to solve the Mathieu equation is by truncating it at some level r_0 . The accuracy of the solution depends on the ratio of the potential and kinetic terms at level r_0 (In the case of Eq. (3.15), the ratio of $E - \Lambda_{2_t}$ and the remaining sum on the third level of the extended fraction.).

It is well known that the truncation method to solve the Mathieu equations is very efficient. But in the case of Eq. (3.15) it might not be so, because of the spatial dependence of coefficients.

It is interesting to compare the above numerical method with the "high temperature" expansion, i.e., the perturbation expansion in powers of β. This

expansion, done up to the third generation in Eq. (3.15), gives for the vacuum energy the following formula:

$$F = N^3 \left(\frac{\beta^3}{24} - \frac{11}{4992} * \frac{\beta^7}{24} + .000162\, \beta^{11}\right), \tag{3.24}$$

where n is the size of the lattice.

Very similar expansion can be done for the first excitation . The difference between the vacuum energy and the first excitation gives the value of the mass gap:

$$m = \frac{6}{\beta} - \frac{71}{105} * \frac{\beta^3}{8}. \tag{3.25}$$

Both Eqs. (3.24,25) can be equivalently derived from the standard perturbation theory in the Hamiltonian formalism.

The high temperature expansion leads to similar truncation in Eq. (3.15) as the method to solve Mathieu equation – indeed, each new "floor" of the fraction contributes an additional power of β^2. However, the "high temperature" series for the Mathieu equation has only a finite convergence radius due to complex singularities, whereas the same truncation followed by the exact solution of the truncated equation can produce numerical results with arbitrary preassigned accuracy for any value of β, if only r_0 is chosen appropriately.

The lesson from the Mathieu equation is that the high temperature expansion might be a good guide as far as the relevant configurations are concerned.One may try to perform the indicated truncations ($r<r_0$ in the Mathieu case, loops σ of size $\sigma<\sigma_0$ in the Yang–Mills case) – but then to solve as precisely as possible the truncated system, instead of power expanding and facing usual convergence problems.

3.3 Computer Program to Produce States and Calculate Matrix Elements.

The computer program produces states generation after generation using the algorithm described in the previous sections, (i.e., by acting with the operator V on the lattice). Each new state is checked against a current list of states. If the state is distinct from those already on the list, it is added to the list; otherwise, it is forgotten. In both cases, the contribution to the coefficient $<(n+1)_k \mid V \mid \tilde{n}_l>$, "on line" with generating states, is calculated using the formula from Appendix B. Thus, the computer program, calculates also all numbers which are needed in Eq. (3.15).

The program was implemented in sequential version on a VAX11/780 and in parallel version on Mark II (5 MHz) Caltech/JPL hypercube [14]. We present the parameters of the sample program, producing states up to the third generation on 4^3 lattice in Appendix C.

3.3.1 The Sequential Implementation.

The exact algorithm implemented on sequential the machine is

1. Generate a new state
2. Compare state with current list
3. If state is distinct from those already on list, add it to list; otherwise, return to step 1.

One can abstract this as a data base problem by mapping the steps into:

1. Generate a data base query
2. Examine data base to see if query satisfied. We define success to be that state (record) already exists; failure that state is new.

3. Add new record to data base if query fails; otherwise, return to step 1.

The data base consists of a set of records with one record per state.

The performance of the algorithm on the concurrent processor will naturally depend on such parameters as the size of the data base; time taken to generate query; time taken to compare the candidate state (query) with a single record in the data base. Thus the design of the concurrent algorithm must be based on the specific problem at hand. We consider here a particular example, namely, the production of the third generation (k=3) of states for a $4 \times 4 \times 4$ lattice.

3.3.2 Concurrent Implementation

This subsection describes the implementation on the Caltech Mark II hypercube which consists of 32 8086-8087 based nodes with the 5-dimensional hypercube geometry. The system has a separate 8086 based controller in which the control process runs. The algorithm does not depend on the particular machine architecture and will work well on any MIMD architecture with large grain size (reasonable memory per node) and ability to send messages between processors. Suppose we have a total of N nodes in the concurrent processor (excluding the control processor).

The problem is decomposed in a simple fashion storing N equal fractions (1/N) of the data base in each node. The algorithm is as follows:

1a) Control process sends to each processor the information necessary to generate the next group of states or in our more general language a group of queries. These 20-30 queries correspond to actions of the operator V on all second generation states.

Each node empties its message buffer and accepts the message from control process.

1b) In each node, we loop over queries in this group.

2a) Each query is first checked to see if it is referenced in a message buffer corresponding to another processor, having found it in its local data base. (See steps 3a, c).

2b) If this check fails, we compare queries with the records currently stored in a given node. This is identical to sequential algorithm but corresponds to a data base that is 1/N of the size.

3a) If the query is successful, a message is sent to all processors indicating this so that they may terminate consideration of a query corresponding to this state.

3b) If the query is unsuccessful, the node either moves to the next one or stores record corresponding to a new state if a simple hashing algorithm determines that this new record (state) is to be stored in this particular node's data base.

3c) At any time, messages may be received from another processor. This message can concern either the current query, a query already considered or a future query. In the first two cases, appropriate action is taken – which might require deletion from the data base of a past state whose query failed in the current node but which was later found in a data base stored in another node. If the message concerns a future state, it is stored in a buffer to be used in step 2a).

3d) A message is sent to control process when the node finishes the given group of queries. When the control process receives N such completion messages, it moves on to the next group.

The steps above are labeled so that, for instance, 1a and 1b of the concurrent algorithm correspond to step 1 of the sequential case in Section 3.

Essential features of the concurrent algorithm are

- The generation of states (queries) is done in every node; i.e., no concurrency is achieved in this step.
- The nodes operate asynchronously on groups of queries and so achieve approximate load balancing that averages over fluctuations in query comparison time.
- A message is sent as soon as a query succeeds in a given node, and the other nodes can therefore immediately terminate any current or future comparison of this query.
- The algorithm not only uses in an essential fashion a general message passing system but also ensures that receipt of a message interrupts the node processor. This is necessary to easily process possible termination of current query. The relevant software was built in terms of the message passing operating system IDOS built internally at Caltech [15].

We ran the concurrent algorithm on the 32 node machine, producing states up to the third generation on the 4^3 lattice. We found that the program ran with the efficiency of 60%. Clearly, the algorithm will perform better as the size of the data base increases. In Appendix D we present the full analysis of the performance of the algorithm.

3.4 Problems with the Linear Approach.

The Eq. (3.15) can be used to calculate exactly (not through the β expansion) the vacuum energy and the mass gap. In Fig. 10, we plot a typical solution. The straight line in this picture represents the left–hand side of the Eq. (3.15). All the other curves correspond to the right–hand side of the Eq. (3.15) plotted as a function of energy E. The interesting value (mass gap) is given by the difference between points b and a.

This approach has two problems which will now be explained. The vacuum energy must be proportional to the volume of the lattice. In Eq. (3.15), the first numerator $<0|V|\tilde{1}><1|V|0>$ is proportional to N^3 as expected, which implies that the whole denominator in 3.15 should be of order of 1 (N independent). It is possible only if the huge $O(N^3)$ numbers: E and the rest of the fraction cancel out to constant terms. In numerical calculations the fraction 3.15 is truncated somewhere. This introduces an error, which can spoil the whole calculation, unless the truncation is done for a high enough generation. Calculations for very high generations are impossible because of the large number of produced states (up to the third generation, on the 4*4*4 lattice, the number of states is 820, but in the fourth generation, on the same lattice, the number of states rises to 40000). That is why the cancellation should be done exactly and analytically.

The second problem, related also to the first one, is that the distance between the numbers a and b in Fig. 10 is very small and it goes to 0 when β increases. We face the same difficulty as before: two huge $O(N^3)$ numbers cancel, when subtracted up to a constant term, being the actual result (mass gap).

Within the formalism developed in the next chapter, the above mentioned difficulties are removed since all volume effects are canceled analytically. The Schrodinger equations to be solved are finite; i.e., they contain only N independent terms.

4.Factorization.

4.1 An Intuitive Explanation of Factorization.

At the end of the last chapter it was pointed out that the linear approach has troubles with cancellations of the volume effects. This cancellation can be done analytically using the ansatz for the wave functions, motivated by the cluster expansion techniques in statistical physics. The method will be first described intuitively on the simplest example of states up to the second generation.

We divided these states into two groups (Fig. 11). The first one consists of states which are single loops of electric flux. The second one is the set of two plaquette[1] states. The operator V_p acting on one plaquette state may produce a single–loop state (with the transition amplitude $1/2$) or a two–plaquette state. In the latter case the transition amplitude is $\sqrt{3}/2$ if the plaquettes touch each other and 1 otherwise.

In the previous chapter each state from the second generation has its own coefficients in the formula (3.3). For states that are loops this will not change. But for states that consist of two plaquettes, the wave coefficient f_{2_i} can be decomposed in the following way:

$$f_{2_i} = f_1 f_1 + \tilde{f}_{2_i} . \tag{4.1}$$

The Eq. (4.1) is based on the assumption that the state 2_i consists mainly of two independent plaquettes. The second term in Eq. (4.1) takes into account that the plaquettes interact when touching each other. The coefficient $\tilde{f}_{2_i}$, called the connected wave function, is expected to decrease exponentially with the distance between plaquettes.

[1] In this chapter we will use the word plaquette to describe the smallest loop on the lattice with representations 1/2 on its links.

The ansatz idea is to rewrite Eqs. (3.10) to (3.12), decomposing the functions f_{2_i} as in Eq. (4.1) and performing analytically the cancellations of disconnected pieces (like $f_1 f_1$ in Eq. (4.1)). In consequence, we get rid of all volume effects and we obtain the system of equations for (finite) connected amplitudes $\tilde{f}_i$. Because, in general, the functions $\tilde{f}$ are smaller than f , neglecting them in the last equations introduces a smaller error than the negligence of the corresponding f functions. This is one of the advantages of factorization. The same type of factorization can be made for states with an arbitrary number of plaquettes. The general formula for factorization will be shown in the next section.

We illustrate the procedure on a simple example of the first two equations (functions f_0 and f_1). Equation (3.10) has the form:

$$<0|\sum_g V|1,g>f_1 = E\ f_0\ . \tag{4.2}$$

The coefficient $<0|\sum_g V|1,g>$ is equal to $3N^3$, because operator V_p, acting on the empty space gives a one–plaquette state with coefficient 1, and the sum over g goes over all plaquettes on the lattice. Thus, the Eq. (4.2) can be rewritten to the form:

$$Mf_1 = E\ . \tag{4.3}$$

In the last equation $M = N^3$, and f_0=1.

The Eq. (3.11) has the form:

$$\Lambda_1 f_1 + <1|V|0> f_0 + \sum_i f_{2_i} <1|V \sum_g |2_i,g> = E\ f_1\ , \tag{4.5}$$

which can be simplified to the form :

$$\Lambda_1 f_1 + 1 + \sum_i <1|V \sum_g |2_i,g> f_{2_i} = E\ f_1\ . \tag{4.6}$$

Using the ansatz (4.1) for the function f_{2_i} one gets the formula :

$$\Lambda_1 f_1 + 1 + \sum_i <1|V\sum_g|2_i,g>f_1 f_1 + \sum_i <1|V\sum_g|2_i,g>\tilde{f}_{2_i} = Ef_1 . \qquad (4.7)$$

In the last equation the terms Ef_1 and $\sum_i <1|V\sum_g|2_i,g>f_1 f_1$ are proportional to the volume, whereas the term $\sum_i <1|V\sum_g|2_i,g>\tilde{f}_{2_i}$ is finite (connected amplitude).

The states contributing to the coefficient $\sum_i <1|V\sum_g|2_i,g>f_1 f_1$ can be divided into two groups. The first one contains all states in which two plaquettes touch each other (Fig. 11). For these states, the coefficient that arises when the operator V_p acts on them is either $1/2$ when the state is a loop, or $\sqrt{3}/2$ if a state consists of two independent plaquettes. All these states are confined to the finite volume around state $<1|$. The volume contains 33 plaquettes (Fig. 12b), and it will be denoted by Ω_1. All other states (i.e. those with disconnected plaquettes), contribute the coefficient 1 multiplied by $M-\Omega_1$ (the volume of the lattice excluding the plaquette positions in which the coefficient is $\sqrt{3}/2$). Thus, the term $\sum_i <1|V\sum_g|2_i,g>$ can be written as :

$$\sum_i <1|V\sum_g|2_i,g>f_1 f_1 = \sum_{g\in\Omega_1}\sum_i <1|V|2_i,g>f_1 f_1 + (M-\Omega_1)f_1 f_1 , \qquad (4.8)$$

or

$$\sum_i <1|V\sum_g|2_i,g>f_1 f_1 = \sum_i\sum_{g\in\Omega_1}(<1|V|2_1,g> - 1)f_1 f_1 + Mf_1 f_1 . \qquad (4.9)$$

Combining Eqs. (4.7) and (4.9) one gets:

$$\Lambda_1 f_1 + 1 + \sum_i\sum_{g\in\Omega_1}(<1|V|2_i,g> - 1)f_1 f_1 \qquad (4.10)$$

$$+ \sum_i <1|V\sum_g|2_i,g>\tilde{f}_{2_i} + Mf_1 f_1 = E\, f_1 .$$

From the Eq. (4.3) $E = Mf_1$, thus terms $Mf_1 f_1$ and Ef_1 cancel each other. Finally,

the Eq. (4.10) takes form:

$$\Lambda_1 f_1 + 1 + \sum_i \sum_{g\in\Omega_1} (<1|V|2_i,g> - 1) f_1 f_1 + \sum_i <1|V \sum_g |2_i,g> \tilde{f}_{2_i} = 0 \,. \quad (4.11)$$

As seen, all large volume effects disappeared: the disconnected piece $f_1 f_1$ is to be summed only over the finite "excluded volume".

It should be pointed out here that the above factorization procedure changes the system of linear equations into the nonlinear one. The generalization of the above procedure will be presented in the next section.

The second problem of the linear approach encountered in the preceding chapter is the difficulty in distinguishing two different solutions of the Mathieu equation. The way to solve this problem is to write separate equations for the mass gap. Solution of this problem will be again intuitively explained on the example of equations for the first two functions.

The Eq. (4.3) for the first excitation can be written in the following form:

$$M f_{G_1} = \Omega_G F_0 \,, \quad (4.12)$$

where the subscript G denotes the first excitation and Ω_G – its energy. The function F_0 is the high temperature vacuum component of the glueball wave function.

The Eq. (4.5) for the glueball takes the form :

$$\Lambda_1 f_{G_1} + F_0 + \sum_i f_{G_{2_i}} <1|V \sum_g |2_i,g> = \Omega_G f_{G_1} \,. \quad (4.13)$$

In the glueball case, the factorization of the wave function starts from the one plaquette amplitude:

$$f_{G_1} = f_1 F_0 + F_1 \,. \quad (4.14)$$

In the last equation capital F stands for coefficients of the factorized wave

functions and f_1 is the coefficient for one plaquette state in the vacuum. An intuitive explanation of Eq. (4.14) is that the plaquette in the glueball can either be a plaquette from the vacuum (coefficient $f_1 F_0$) and the glueball is in the ground state, or a plaquette from the glueball (coefficient F_1) and the vacuum is in the ground state.

Very similar factorization is carried out for two plaquette states :

$$f_{G_{2_t}} = F_{2_t} + 2f_1 F_1 + F_0 f_{2_t} . \tag{4.15}$$

In the last equation the first coefficient (F_{2_t}) tells that both plaquettes are from a glueball. The second ($2f_1 F_1$) states that one is from the vacuum and the other one from the glueball. The last coefficient ($F_0 f_{2_t}$) tells that both plaquettes are from the vacuum. The factorization for two–plaquette loops is the same as for one plaquette.

Combining Eqs. (4.12) and (4.14) one gets :

$$M f_1 F_0 + M F_1 = \Omega_G F_0 . \tag{4.16}$$

From the Eq. (4.3) $M f_1 = E$; thus,

$$M F_1 = (\Omega_G - E) F_0 . \tag{4.17}$$

The difference $\Omega_G - E$ (energy of the first excitation minus vacuum energy) is the mass gap and it will be denoted by m_G. The Eq. (4.17) can be rewritten to the form :

$$M F_1 = m_G F_0 . \tag{4.18}$$

Combining Eqs. (4.13,15) one gets:

$$(\Lambda_1 - \Omega_G)(f_1 F_0 + F_1) F_0 + \sum_l (f_{2_t} F_0 + F_{2_t}) \langle 1 | V \sum_g | 2_l, g \rangle \tag{4.19}$$

$$+ \sum_i (F_{2_t} + 2_1 F_1 + F_0 f_{2_t}) \langle 1 | V \sum_g | 2_i, g \rangle = 0 ,$$

where subscript 2_l refers to states with two plaquette loops.

In the Eq. (4.19) one can separate the following part :

$$F_0((\Lambda_1-\Omega_C)f_1+1+\sum_l f_{2_l}\langle 1|V\sum_g|2_l,g\rangle+\sum_i f_{2_i}\langle 1|V\sum_g|2_i,g\rangle)\,. \qquad (4.20)$$

This part is the vacuum Eq. (4.6) with E substituted by Ω_C . Thus, the whole (4.20) part equals :

$$F_0(E-\Omega_C)f_1 = -F_0 m_C f_1\,. \qquad (4.21)$$

Taking into account (4.18) the (4.20) part can be simplified to :

$$F_0(E-\Omega_C)f_1 = -MF_1 f_1\,. \qquad (4.22)$$

Thus the Eq. (4.19) takes the form:

$$-Mf_1F_1+(\Lambda_1-\Omega_C)F_1+\sum_l F_{2_l}\langle 1|V\sum_g|2_l,g\rangle \qquad (4.23)$$

$$+\sum_i(F_{2_i}+2f_1F_1)\langle 1|V\sum_g|2_i,g\rangle = 0.$$

In Eq. (4.23) the coefficient $\sum_i 2f_1F_1\langle 1|V\sum_g|2_i,g\rangle$ can be treated in the same way as in Eq. (4.9), which gives:

$$2f_1F_1\sum_i\langle 1|V\sum_g|2_i,g\rangle = 2f_1F_1\sum_i\sum_{g\in\Omega_i}(\langle 1|V|2_i,g\rangle-1)+2Mf_1F_1\,, \qquad (4.24)$$

where Ω_1 is the volume (33 plaquettes) around state $\langle 1|$. Thus, the Eq. (4.23) can be written as :

$$(\Lambda_1-\Omega_C)F_1+\sum_l F_{2_l}\langle 1|V\sum_g|2_l,g\rangle+\sum_i F_{2_i}\langle 1|V\sum_g|2_i,g\rangle \qquad (4.25)$$

$$+2f_1F_1\sum_i\sum_{g\in\Omega_i}(\langle 1|V\sum_g|2_i,g\rangle-1)+Mf_1F_1=0\,.$$

In Eq. (4.25), the term Mf_1F_1 can be combined with the term $-\Omega_C F_1$. From the

vacuum Eq. (4.3) $Mf_1=E$. The above two terms give $-m_C F_1$. The final form of the first equation for the glueball is then:

$$\Lambda_1 - m_C + \sum_l F_{2_l} <1|V \sum_g |2_l,g> + \sum_i F_{2_i} <1|V \sum_g |2_i,g> \qquad (4.26)$$

$$+ 2f_1 \sum_i \sum_{g\in\Omega_i} (<1|V \sum_g |2_i,g> - 1) = 0 .$$

The normalization in the last equation is chosen so that $F_1=1$. This choice is convenient for comparing results with the high temperature expansion. The Eq. (4.26) does not contain any coefficients that are of the order of the size of the lattice. The coefficient $\sum_i F_{2_i} <1|V \sum_g |2_i,g>$ is small because F_{2_i} exponentially decreases when the distance between plaquettes increases. Equations for higher functions can be constructed in a similar way.

4.2 Numerical Results for the Glueball Mass Using the Simple Formalism of Factorization.

In the similar way as in the previous section we derived the equations to calculate the glueball mass numerically . All required numerical coefficients were produced by the computer program described in Chapter 2. The calculations were carried out up to states with correlation length less than 3. The states taken into account were those which have at most three plaquettes different from zero and such that the biggest distance between separate plaquettes was "a" (one lattice spacing). Examples of such states are shown in Fig. 15.

To get the mass gap for a given β, first the vacuum equations for functions $\tilde{f}$ were solved. Then the functions $\tilde{f}$ were used as input in the equations for glueball and functions F and m_C were calculated. The calculations were made for β ranging from 1 to 2.25. The results are shown in Fig. 16,17.

In Fig. 16 we plotted the logarithm of the mass gap versus β. The line 1 presents scaling formula (1.29) for the physical mass, with the value of the

lattice mass calculated in Monte–Carlo method. The shaded area shows the shift of the line 1 due to statistical errors in the Monte–Carlo technique. Our results for the glueball mass, in different approximations, are presented by curves 3–5. The line 3 is the value of the mass calculated using only the loops from the second generation. The curve 4 shows results which contained all loops up to the third generation. The line 5 was obtained by also including two plaquette states. For comparison we also plotted the mass gap obtained from the high temperature formula (3.25) (curve 2).

The Fig. 16 shows that the solution in our semianalytic technique improves when including more and more states. The slope of the line 5 in the region of change β between 1.8 and 2 is close to the slope of the line 1. The result for the glueball mass is in the range 120 – 200 (170 ± 30 from Monte–Carlo).

In Fig. 17 we plotted the values of the wave function coefficients versus β for different types of states. The picture shows definite hierarchy between states. The coefficient of the plaquette is always bigger then for any other loop. This confirms that neglecting bigger loops is legitimate.

In all performed calculations the dominant part of the result for m_G came from terms in equations such as $2f_1\sum_i \sum_{g\in\Omega_1} (<1\,|\,V\,|\,2_i,g>-1)$, a term in Eq. (4.26).

4.3 The General Formalism of Factorization.

The general formalism of factorization is constructed in the electric flux loops basis. In this basis one can introduce raising $L_\sigma^+(g)$ and lowering $L_\sigma(g)$ operators.The operator $L_\sigma^+(g)$ acting on state $|\psi>$ adds to it an electric flux loop of shape σ and in position g. The operator $L_\sigma(g)$ subtracts the loop. The $g=(R\,|\,n)$ is a pair of:

n lattice vector specifying loop position,

R cubic rotation, describing the geometrical orientations of the loop, with one point fixed at n.

Physical states containing one, two, etc. loops, injected into the high temperature vacuum (empty network) are denoted as follows:

$$|\sigma,g>,\ |\sigma_1\sigma_2,g_1g_2>,\cdots$$

where σ's describe different loop shapes.

For every one-loop state one introduces a vacuum wave function coefficient f_σ. For every two-loop state the wave function coefficient is the connected function $\tilde{f}_{\sigma_1\sigma_2}(g_1,g_2)$ where σ_1 is the shape of the first loop and σ_2 is the shape of the second loop. The g_1 and g_2 denote the positions of loops in space. In general, the connected wave function coefficient for a n-loops state is $\tilde{f}_{\sigma_1\cdots\sigma_n}(g_1\cdots g_n)$.

With the above definitions one can define operator Γ as follows:

$$\gamma^+ = \sum_\sigma f_\sigma \sum_g L^+_\sigma(g) + \frac{1}{2}\sum_{\sigma_1\sigma_2}\sum_{g_1g_2}\tilde{f}_{\sigma_1\sigma_2}(g_1,g_2)L^+_{\sigma_1}(g_1)L^+_{\sigma_2}(g_2)+\cdots . \qquad (4.27)$$

$$\Gamma = \gamma^+ - \gamma \qquad (4.28)$$

The definition 4.27 is very similar to the definition of operator W generating connected graphs in the conventional field theory. As in the perturbative case all graphs are generated by exponentiation of Γ. Thus, the operator which creates all states on the lattice is e^Γ. This operator acting on the empty lattice (state $|0>$) produces the exact vacuum state $|\dot{0}>$ as follows:

$$|\dot{0}> = e^\Gamma|0> . \qquad (4.29)$$

The state $|\dot{0}>$ is our ansatz for the exact physical vacuum. The requirement of the translational and rotational invariance of the vacuum state essentially restricts the possible g dependence of the loop amplitudes. We have

$$f_\sigma(g) = f_\sigma \,, \quad (\, g \; independent \,) \,, \tag{4.30}$$

$$\tilde{f}_{\sigma_1\sigma_2}(g_1, g_2) = \tilde{f}_{\sigma_1\sigma_2}(g_1^{-1} g_2) \,, \quad etc. \tag{4.31}$$

Since the $|\dot{0}>$ state is an eigenstate of the Hamiltonian, then

$$H\,|\dot{0}> = E\;|\dot{0}> \,. \tag{4.32}$$

The E is the vacuum energy. Definition (4.27) assures that the norm is preserved:

$$<\dot{0}\,|\,\dot{0}> \;=\; <0\,|\,0> \;=\; 1 \,. \tag{4.33}$$

Combining Eqs. (4.29) and (4.32) one gets

$$H\, e^{\Gamma}|0> = E\;\; e^{\Gamma}|0> \,, \tag{4.34}$$

or

$$\hat{H}\,|0> = E\,|0> \,, \tag{4.35}$$

where

$$\hat{H} \;=\; e^{-\Gamma} H\; e^{\Gamma} \,. \tag{4.36}$$

For the zero momentum 0^{++} state (glueball) one introduces operator X^+ :

$$X^+ = \sum_\sigma F_\sigma \sum_g L^+_\sigma(g) + \frac{1}{2} \sum_{\sigma_1\sigma_2} \sum_{g_1 g_2} F_{\sigma_1\sigma_2}(g_1, g_2) L^+_{\sigma_1}(g_1) L^+_{\sigma_2}(g_2) + \cdots \,. \tag{4.37}$$

In Eq. (4.37) functions F are the connected wave function coefficients for the glueball. Operator X^+ acting on the perturbative vacuum state $|0>$ produces glueball state $|G>$:

$$|G> \;=\; e^{\Gamma} X^+ |0> \,, \tag{4.38}$$

or

$$|G> = e^{\Gamma} X^{+} e^{-\Gamma} |\dot{0}> . \tag{4.39}$$

The intuition behind this construction is very simple. The operator e^{Γ} simply pumps loops of electric flux into the empty network in all possible ways. The singlet conditions assure that the resulting medium is globally homogeneous, with "local" fluctuations described by the loop amplitudes. How local they are depends on the actual correlation length, or, equivalently, on the characteristic loop size.

The operator $X^{+}(g)$ generates local inhomogeneity by injecting extra loop (or loops) around g . The operator e^{Γ} assures that the medium far from the glueball looks exactly as in the vacuum. The zero momentum 0^{++} condition imposes the same restrictions on the glueball loop amplitudes; i.e., the local inhomogeneity might happen everywhere in space with the same probability.

The state $|G>$ is the first excitation eigenstate of the Schrodinger equation:

$$H |G> = \Omega_G |G> , \tag{4.40}$$

where Ω_G is the first excitation energy. Taking into account 4.38 and 4.40 one gets :

$$e^{\Gamma} \hat{H} X^{+} |0> = e^{\Gamma} ([\hat{H}, X^{+}] + X^{+} \hat{H}) |0> = \tag{4.41}$$

$$= e^{\Gamma} ([\hat{H}, X^{+}] + X^{+} E) |0> = \Omega_G e^{\Gamma} X^{+} |0>,$$

or

$$[\hat{H}, X^{+}] \; |0> = m_G X^{+} |0> . \tag{4.42}$$

Denoting $\hat{X} = e^{-\Gamma} X e^{\Gamma}$ the Eq. (4.42) takes the following form:

$$[H, \hat{X}^{+}] \; |\dot{0}> = m_G \hat{X}^{+} |\dot{0}> . \tag{4.43}$$

Both Eqs. (4.35) and (4.43) can be used to produce an infinite set of

equations for the vacuum energy E and the mass gap m_G.

Taking the scalar product of Eq. (4.35) with state <0|, one gets:

$$<0|\hat{H}|0> = E \ . \tag{4.44}$$

This is the only equation that contains explicitly the size of the lattice and that can be produced from Eqs. (4.35) and (4.43). In all other equations the lattice size dependence is factored out by operators $\hat{H}$ and $\hat{X}$ and commutator $[H,\hat{X}]$. It is the general way of factorization of the volume effects.

So far the whole formalism is completely general. To proceed further, we try to follow intuitions coming from the analysis of the Mathieu equation. The high temperature expansion would suggest:

$$\tilde{f}_{\sigma_1\sigma_2} \ll \tilde{f}_{\sigma} \ll 1 \ , \tag{4.45}$$

i.e., small loop density and negligible correlations. One may therefore try the ansatz (4.45) without power expanding. In other words, we say that the loop density is small, correlations marginal, but nothing is expected to be analytic in β .

Instead of β, we use the loop amplitudes f_σ as expansion parameters. Expansion of the effective Hamiltonian $\hat{H}$

$$\hat{H} = H - [\ \Gamma,H\ ] + \frac{1}{2}[\ \Gamma,[\ \Gamma,H\ ]\ ] + \cdots \tag{4.46}$$

generates a series of connected "local" n–loop vertices, where "local" means that the non–zero contribution from the nested commutator comes only from the loop configurations with at least one common plaquette, touching all n loops.

The simplest vertices emerging in the expansion are

$$P_{\sigma\tau} = \frac{1}{\Omega} <\sigma|[\ \tau^+,P\ ]|\ 0> \ , \tag{4.47}$$

$$J_{\sigma,\tau_1\tau_2} = \frac{1}{\Omega} <\sigma|[\ \tau_1^+,[\ \tau_2^+,P\ ]\ ]|\ 0> \ , \tag{4.48}$$

$$I_{\sigma_1\sigma_2,\tau_1\tau_2} = \frac{1}{\Omega}\left(<\sigma_1\sigma_2|\tau_1\tau_2> - \Omega^2(\delta_{\sigma_1\tau_1}\delta_{\sigma_2\tau_2} + \delta_{\sigma_1\tau_2}\delta_{\sigma_2\tau_1}) \right), \qquad (4.49)$$

where Ω = volume of the space group S = 48 × space volume. The states $|\sigma>$, $|\tau>$ etc. are obtained from $|\sigma,g>$, $|\tau,g>$ by summing over all loop positions g. The normalization is $<\sigma|\tau> = \delta_{\sigma\tau}\,\Omega$.

The quantity $P_{\sigma\tau}$ is the single loop deformation amplitude: loop τ, deformed by the plaquette operator P goes into loop σ. We derive it using formula from Appendix B and multiplying the resulting product of the Wigner symbols by appropriate geometric factors.

To derive the vertex $J_{\sigma,\tau_1\tau_2}$, one expands commutators and, using the fact that single loop states are always orthogonal, one gets

$$J_{\sigma,\tau_1\tau_2} = \frac{1}{\Omega}\left(<\sigma|P|\tau_1\tau_2> - \Omega^2(\delta_{\sigma\tau_1}\delta_{\tau_2 1} + \delta_{\sigma\tau_2}\delta_{\tau_1 1}) \right), \qquad (4.50)$$

where $\tau = 1$ is the plaquette loop. There are two typical contributions to the vertex J: one comes from the decay process Fig. 12c; the other one, present only for non–Abelian groups, is due to the touching interactions. E.g., consider the case $\tau_1 = \sigma \neq 1$, $\tau_2 = 1$. The result is

$$J_{\sigma,\sigma 1} = \left(\frac{\sqrt{3}}{2} - 1 \right) \times \textit{geometrical factor} \ .$$

Hence, the connected amplitude for creating a plaquette from the vacuum in the "external field" of the loop σ is always negative. The factor $\frac{\sqrt{3}}{2}$ comes from touching (see Fig. 12b), whereas the subtraction is due to the fact that the commutator measures only the departure of a given transition from the factorized value. A new plaquette can be created anywhere in space with unit amplitude and this trivial ("infrared") singularity is subtracted in Eq.4.50. The subtraction affects, however, the final value as well. Intuitively, we may say that the loop σ repels the plaquette. This repulsive force turns to be of crucial numerical importance.

The interaction $I_{\sigma_1\sigma_2,\tau_1\tau_2}$ is due to the loop zero modes. Indeed, as seen from Eq.(4.49), I measures the departure from the uniqueness of the loop decomposition. Non–zero contributions come, e.g., from the loop configurations of Fig. 12a Hence, the effect of loop zero modes can be represented by additional interaction vertices (with four or more external loop lines).

As usual in the case of connected Green's function expansions, one can formulate the diagrammatic interpretation (Feynman rules) of the resulting formula. Pictorial conventions are presented in Fig. 13 . The loop potential v_σ is given by

$$v_\sigma = 3 \times loop\ length\ (in\ lattice\ units\ ) . \tag{4.51}$$

All higher vertices appearing in Eq.(4.46) are of I or J form with an increasing number of external lines; e.g., $J_{\sigma_1\sigma_2,\tau_1\tau_2}$ in Fig. 13 is given by

$$J_{\sigma_1\sigma_2,\tau_1\tau_2} = \frac{1}{\Omega}<\sigma_1\sigma_2|[\,\tau_1^+,[\,\tau_2^+,H\,]\,]|\,0> . \tag{4.52}$$

The Schrodinger Eqs. (4.35,42) are presented in Fig. 14a. They have the form of an infinite coupled system of Bethe–Salpeter–type equations with calculable vertices and with differentiation (kinetic term) replaced by loop deformation.

4.4 Calculations up to 3 Correlation Length.

The "Mathieu method" for solving this system, where we try to mimic the procedure of building the infinite fraction, is the following. First, following the finite loop density ansatz, we neglect all n–loop correlation functions for n > n_0 (n_0 = ?). Then we proceed recursively, iterating equations downward, i.e., expressing always more complicated correlations (with larger n) by simpler functions, to end up with effective "renormalized" equations for one loop amplitudes $\tilde{f}_\sigma, \tilde{F}_\sigma$. E.g., for $n_0 = 2$ the procedure is as in Fig. 14a. We first derive two–loop functions $\tilde{f}_{\sigma_1\sigma_2}, \tilde{F}_{\sigma_1\sigma_2}$, as indicated in Fig. 14b and we insert the result into

the first equation. We get one–loop equations with the Feynman loop corrections, renormalizing the deformation amplitudes $P_{\sigma\tau}$ (in the vacuum, we also get J vertex renormalization at this order) – see Fig. 14c.

Hence, by varying n_0 we can control the renormalization effects "from the top". Starting at $n_0 = 1$ with only the global contours of the bound state, sketched by the loop shapes, we can then go inward, asking for more and more granular structure, with n_0 tuned appropriately to the size of external probe. The renormalization effects organize indeed in the form of an infinite fraction, with the Mathieu nested denominators being the energy denominators in the nested loop corrections. It is quite opposite to the conventional renormalization in continuum theory, where we start "from the bottom" with so detailed a microscopic description that we do not see bound states at all.

Technically, the Feynman loops diagrams are as they always are: momentum integrals over some energy denominators, in our case given by the spectrum of the "bare" single loop Hamiltonian $H_{\sigma\tau}$ (corrected for the scattering effects) – see Fig. 14c . Loops propagate by a chain of successive deformations. The calculations are, however, more complicated than in conventional perturbation theory since, when dealing with the extended virtual objects (loops), we have to sum both over translational and rotational degrees of freedom and over the full spectrum of $H_{\sigma\tau}$.

We tried first the simplest case $n_0 = 1$; i.e., we have neglected all correlations. In principle, there is nothing that prevents more extensive calculations – in particular we have already worked out all necessary rules for dealing with loop–loop diagrams, based on the representation theory of the lattice symmetry group. Everything is calculable – it is just a matter of human and computer time.

The explicit form of the equations we used is:

vacuum energy density:

$$\frac{E_o}{\Omega} = \frac{1}{4}\tilde{f}_1 - \frac{1}{2}\left(J_{\tau_1,\tau_2\tau_3} + \frac{1}{12} I_{\tau_1\tau_2,\tau_3 1} \right)\tilde{f}_{\tau_1}\tilde{f}_{\tau_2}\tilde{f}_{\tau_3} + \cdots \tag{4.53}$$

vacuum equations:

$$\frac{\upsilon_\sigma}{\beta^2}\tilde{f}_\sigma = \frac{1}{4}\delta_{\sigma 1} + P_{\sigma\tau}\tilde{f}_\tau + \tag{4.54}$$

$$+ \frac{1}{2}\left(J_{\sigma,\tau_1\tau_2} + J_{\tau_1,\tau_2\sigma} + J_{\tau_2,\tau_1\sigma} + \frac{1}{4} I_{\tau_1\sigma,\tau_2 1} \right)\tilde{f}_{\tau_1}\tilde{f}_{\tau_2} + \cdots$$

glueball equations:

$$\left(\frac{\upsilon_\sigma}{\beta^2} - \lambda \right)F_\sigma = \left(P_{\sigma\tau} + E_{\sigma\tau}(\tilde{f}) \right)F_\tau , \quad \lambda = \frac{2}{\beta} m_G , \tag{4.55}$$

$$E_{\sigma\tau}(\tilde{f}) = \left(J_{\sigma,\tau\eta} + J_{\tau,\sigma\eta} + \frac{1}{8}\left(I_{\sigma\eta,\tau 1} + I_{\tau\eta,\sigma 1}\right) \right)\tilde{f}_\eta + \cdots \tag{4.56}$$

(all repeated loop indices are summed over).

The approximations are rather drastic: we have neglected all correlations, and we included only a few powers of $\tilde{f}_\sigma$ (3 for the vacuum density, 2 for vacuum equations, 1 for the glueball Hamiltonian). The point, however is that, even with so naive input, we get on return some non–trivial information about the non–Abelian loop dynamics.

We solve Eqs. (4.53,56) as follows:

a) loop basis is generated and truncated at a certain value of σ_0 = surface in lattice units. The actual calculations were performed with all loops up to σ_0 = 3. There is one loop with σ_0 = 1 (plaquette), 4 loops with σ_0 = 2, 34 loops with σ_0 = 3. We draw all of them in Fig. 15 .

b) deformation amplitudes P and vertices I, J are derived, partially analytically (SU(2) content), partially numerically (geometrical multiplicity factors due to the loop shapes by computer program).

c) the vacuum equations are solved numerically. It is a system of 39 nonlinear inhomogeneous equations, with, however, rather moderate nonlinearity (loop amplitudes $\tilde{f}$ are small). We start with the high temperature result for small β ($\beta \approx 0.1$), and then we go in small steps in β, using the standard iteration method (matrix Newton with the solution at given β used as input for the next step). The convergence is very fast.

d) using the derived vacuum loop amplitudes we calculate and diagonalize the effective glueball Hamiltonian (Eq. (4.56)). We then select the smallest eigenvalue and, starting in the cross–over region, we look for the scaling signal

$$m_0(\beta) = \mu_0 \beta^{\gamma_0} e^{-\frac{\beta}{\beta_0}}, \tag{4.57}$$

with β_0 , γ_0 given by the standard weak coupling renormalization group.

This is the basic numerical procedure, which, after adding enough powers of $\tilde{f}$, correlations, quarks, strings, changing SU(2) to SU(3) etc., is expected to return as μ_0 the low energy QCD spectrum.

Our results, in the region $2 < \beta < 2.5$ are as follows:

The loop amplitudes are small, as expected, supporting the ansatz of the dilute loop gas. Typical values for β 2 are : $\tilde{f}_{\sigma_0=1}$ 0.1, $\tilde{f}_{\sigma_0=2}$ 0.05, $\tilde{f}_{\sigma_0=3}$ 0.02.

The mass gap is very sensitive to the vacuum corrections to the effective Hamiltonian. The dominant terms come from the J vertex. The leading contribution is diagonal, i.e., modifying the loop potential:

$$v_\sigma \to v_\sigma^* = v_\sigma - 2\beta^2 \sum_\tau J_{\sigma,\sigma\tau} \tilde{f}_\tau + O(\tilde{f}^2) . \tag{4.58}$$

Since J's are negative, as discussed, potential is increased by the "external field" contributions, which is the similar term to $2f_1 \sum_i \sum_{g\in\Omega_i} (<1|V|2_i,g>-1)$ in Eq. (4.26).

With the correction term switched off, the mass gap vanishes around $\beta = 2$. This seems to be the usual Abelian phase transition: the potential term v_σ and the kinetic term $P_{\sigma\tau}$, being both of order of the loop length, effectively cancel at a certain value of β. The potential is not strong enough to bind the loop size; the entropy of loop deformations wins and the loops blow up.

Now the touching interaction enters. Even if small (proportional to $\tilde{f}_\sigma$), it plays crucial role because of cancellations in the original Hamiltonian. Since the sign of correction is always positive, the touching interaction keeps the mass gap small and positive.

The value of $\mu_o(\beta)$ in Eq. (4.57), expected to be constant ($\mu_o = 170 \pm 30$ from Monte Carlo [12]), actually moves between $100 < \mu_o < 200$, depending on particular approximations (we played with Eqs. (4.53,57), switching on/off various pieces like loop decays, zero modes etc.), to blow up finally to either plus or minus infinity beyond $\beta \approx 2.5$.

We have, nevertheless, learned something. It seems that the "external pressure" due to the touching interaction does the job, stabilizing the loop system, but one should calculate it more precisely than we did. Only the linear term has been included, which is against any numerical rules of the game, once the "correction" turns out to be, in fact, the leading effect.

An optimistic observation is that the loop zero mode contributions (I interaction) are rather marginal, which supports our choice of variables. The reason is purely combinatorial: the ambiguities arise only for special geometrical configurations, whereas touching is much more extensive and geometrically enhanced.

Whether the touching interaction is the mechanism for confinement in our language or just one of many contributions, accidentally dominating in this region, is obviously an open question, requiring more accurate calculations. It is nevertheless amusing that the sign of the effect is well defined, that it switches on in the right beta region and, finally, that, in a similar way as the sign of the beta function, our sign is also negative due to infrared subtraction, just a little bit larger than the original, positive definite quantity. The amplitude for touching is always less than unity, since there is another open channel–deformation ($(\frac{\sqrt{3}}{2})^2 + (\frac{1}{2})^2 = 1$; see e.g., Fig. 12b). This suggests the "Sudakov formfactor" interpretation: the whole effect sums up to unity but, being reshuffled between various energy levels, it generates some kind of unitarity damping for large loop fluctuations in a given level.

5. Conclusions

This work contains the proposal for the semianalytic lattice loop calculus useful in the low–energy sector of the Yang–Mills theory. The formalism can be extended to any $SU(N)$ theory and, in particular, it can be applied for Quantum Chromodynamics, after including quark degrees of freedom. As a first application, the method has been used to calculate the mass gap (0^{++} glueball) in the Yang–Mills theory. The formalism seems to be very promising. It provides both numerical results and some understanding of the dynamics of the gauge fields. The actual numerical value of the glueball mass varied, depending on the approximation, between 100–200 (Compare Monte–Carlo result, 170 ± 30). Our best value of the glueball mass 150, or in physical units 520 MeV[1], is entirely consistent with the Monte–Carlo data (Fig.16). We found that the physical picture for the Yang–Mills vacuum in the cross–over region is that of, still quite dilute, gas of fluctuating loops. The glueball looks in our formalism like a local inhomogeneity in the loop distribution. We made the simplest possible approximation of the glueball, describing it by one extra loop[2] . In the future calculations of the mass gap one should also take into account multiloop elements of the wave function (loop–loop correlations). In our language the mechanism of confinement is provided by the " touching interaction" between loops from the glueball and loops from the vacuum. This looks like an "external pressure" exerted by the vacuum on the glueball state, which is very similar to the external pressure in the Bag Model. The "touching interaction" ("external pressure") prevents the glueball loop from blowing up in the strong → weak coupling transition region (as it would happen in the Abelian theory).

---

[1] The actual value of Λ_{mom} for $SU(2)$ gauge theory is unknown. If one takes Λ_{mom} for $SU(3)$ equal 200 MeV, and uses it to rescale the result, then the value of the glueball mass in "physical units" is 520 MeV.

[2] In the calculations presented in Section 4.2 we also took into account the plaquette–plaquette correlations.

We presented two types of numerical calculations. The first one, simpler and more numerically oriented (Section 4.2), provided the value of the 0^{++} glueball mass in $SU(2)$ gauge theory. This calculation gave some insight into the dynamics of the gauge fields. The intuitive informations we got from it were that:

a) the largest contribution to the mass comes from terms which describe the renormalized interaction between the vacuum and glueball loops (This effect was later identified in the second numerical attempt as the candidate for mechanism of confinement.)

b) the loop amplitudes are small and there exists hierarchy in the loop size (the largest is plaquette and the other loops have an order of magnitude of smaller value), which justifies the cut in the loop size in our calculations.

The second numerical attempt (Section 4.4), more analytic and complete, gave the similar value for the mass gap. It provided us with intuition about the "touching interaction" and the mechanism of confinement. It also gave us better understanding of the importance of different terms in equations (4.53,55). In particular , an optimistic observation was that the loop zero mode contributions (I interactions) are rather small, supporting our choice of loops as variables.

The presented numerical results seem to justify the expansion in terms of the loop amplitudes. The values of the coefficients are small. Typical values of loop amplitudes at $\beta \tilde{} 2$ for loops from the first, second and third generation, respectively, are: $\tilde{f}_{\sigma_0=1} \tilde{} .1$, $\tilde{f}_{\sigma_0=2} \tilde{} .05$, $\tilde{f}_{\sigma_0=3} \tilde{} .02$.

The described numerical calculations were in some parts performed on sequential machine and in other parts on the Caltech/JPL hypercube. In both cases they did not require a long computer time (the longest program was executed in less then half an hour).

The natural way to improve the accuracy of the result is to include into calculations loops up to the fourth generation and to include loop–loop correlation

functions. This task requires a large programming effort. There are three limitations for the possible numerical improvement of the result:

a) Computer memory.

With the present computer memories, of size of a hundred Mbytes, it should be possible to do calculations including loops up to the fifth generation.

b) Computer time.

This criterion is of less significance. Computer time for calculations with loops up to the fifth generation should be about one hundred hours.

c) Human resources.

Programming of this method is a rather tedious task and requires a lot of time. This is the most crucial limitation. It took us about a year of programming effort to produce the current numerical results. Our programs, after some changes, can be used to do calculations with larger loops. However, the complete analysis should also contain the multiloop states, loop–loop correlations, etc. In fact, we have developed the formalism for dealing with loop–loop correlations, but implementing it on the computer is much more complicated than the work for single loops.

Appendix A.

In this Appendix we calculate the coefficients β_r^*(see Eq.(2.11)) for SU(2) group. The character expansion formula takes the form:

$$e^{\beta\chi_s(g)} = \Omega(\beta)[1 + \sum_{i\neq 0} d_i e^{\beta_i^*}\chi_i(g)] , \tag{A.1}$$

where d_i is dimension of representation; χ denotes characters and

$$\Omega(\beta) = \int dg \ e^{\beta\chi_s(g)} . \tag{A.2}$$

Multiplying both sides of (A.1) by $\chi^s(g^{-1})$ and integrating over the whole group, one gets:

$$\int dg\,\chi^s(g^{-1})e^{\beta\chi_s(g)} = \Omega(g)[\int dg\,\chi^s(g^{-1}) + \sum_{i\neq 0} d_i e^{\beta_i^*}\int dg\,\chi^s(g^{-1})\chi_i(g)] . \tag{A.3}$$

The last equation for $s=0$ gives:

$$\int dg\, e^{\beta\chi_s(g)} = \Omega(g) , \tag{A.4}$$

and for $s\neq 0$:

$$\int dg\,\chi^s(g^{-1})e^{\beta\chi_s(g)} = \Omega(\beta)d_s e^{\beta_s^*} \tag{A.5}$$

$$d_s e^{\beta_s^*} = \frac{\int dg\,\chi^s(g^{-1})e^{\beta\chi_s(g)}}{\int dg\, e^{\beta\chi_s(g)}} . \tag{A.6}$$

The $SU(2)$ invariant measure is parameterized by angular variables:

$$\int dg = -N \int dV \int_0^{2\pi} \sin^2\phi \ d\phi . \tag{A.7}$$

The characters are:

$$\chi_l(g) = \frac{\sin((2l+1)\phi)}{\sin\phi} . \tag{A.8}$$

Eqs. A.7 , A.8 and A.6 give:

$$d_l e^{\beta_l^*} = \frac{\int_0^{2\pi} \sin\phi \, sin((2l+1)\phi) e^{2\beta\cos\phi} d\phi}{\int_0^{2\pi} \sin^2\phi \, e^{2\beta\cos\phi} d\phi} . \tag{A.9}$$

Both integrals are calculated using the saddle point method. This gives after some algebra:

$$d_l e^{\beta_l^*} = \frac{e^{-\frac{(l+1)^2}{\beta}} - e^{-\frac{l^2}{\beta}}}{e^{-\frac{1}{\beta}} - 1} . \tag{A.10}$$

Expansion of both sides of Eq.(A.9) leads to :

$$d_l(1 + \beta_l^*) = (2l+1)(1 - \frac{l(l+1)}{\beta}) . \tag{A.11}$$

Finally from Eq. (A.10) one gets:

$$\beta_l^* = - \frac{l(l+1)}{\beta} . \tag{A.12}$$

Appendix B

In this appendix we present the general formula for amplitude P_r^l. Suppose that operator V_p acts on a state characterized by a set of variables $\{l,r\}$ in the xy plane, as indicated by the dashed line in Fig. 20 (the circles in the picture present Clebsch–Gordon vertices as in Fig. 4a). The formula for amplitude P_r^l is the product of four similar expressions around plaquette v_n, so we present only one of them. Let consider the right lower corner of the plaquette. The expression for this vertex is :

$$v_1 = \begin{vmatrix} l'_{y_{1+}} & l_{y_{1-}} & r'_{y_1} \\ r_{y_1} & \frac{1}{2} & l_{y_{1+}} \end{vmatrix} \times \begin{vmatrix} r'_{y_1} & r_{z_1} & r'_{x_1} \\ r_{x_1} & \frac{1}{2} & r_{y_1} \end{vmatrix} \times \begin{vmatrix} l'_{x_{1-}} & l_{x_{1+}} & r'_{x_1} \\ r_{x_1} & \frac{1}{2} & l_{x_{1-}} \end{vmatrix} \times$$

$$\times \sqrt{(2r_{y_1}+1)(2r_{x_1}+1)(2(r_{y_1}+r'_{y_1})+1)(2(r_{x_1}+r'_{x_1})+1)} \times \qquad \text{(B1)}$$

$$\times ((2(l_{y_{1+}}+l_{y_{1-}})+1)(2(l_{x_{1-}}+l_{x_{1+}})+1)(2l_{x_{1-}}+1)(2l_{y_{1+}}+1))^{1/4},$$

where primes denote the change of the value by $1/2$, and r has the same meaning as in picture 4a.

The expression for other vertices is obtained by changing indices in formula (B1). The global formula for P_r^l is then:

$$P_r^l = phase \times v_{p_1} v_{p_2} v_{p_3} v_{p_4}, \qquad \text{(B2)}$$

where $phase$ is :

$$phase = (-1)^{\Delta r_{y_1} + \Delta r_{y_4} + \Delta r_{z_1} + \Delta r_{z_2}}, \qquad \text{(B3)}$$

and

$$\Delta r_n = r'_n - r_n. \qquad \text{(B4)}$$

Appendix C

Table 1: Parameters of a Sample Problem
Production of Third Generation of 4^3 Lattice

Total Execution Time	1300 Seconds 6600 Seconds	(VAX11/780) (Single 8086–87 node of Caltech Hypercube)
Number of Queries (Candidate States)	2571	
Number of Distinct Records (Final number of States)	890	
Fraction of Time Spent on failed queries (new states)	0.62	
Fraction of Time Spent on successful queries (States already on list)	0.36	
Fraction of Time Spent Generating Queries	0.02	
Total number of Data base comparisons	1.06×10^6	
Average number of comparisons for successful queries	412	
Average number of comparisons Comparisons for failed queries	445	

The details of the sample program to produce states are given in Table 1. Note that queries of the data base involve a brute force search through all records, and it was considered impractical to set up special indices (hashing) to speed up the search. In the case of successful queries (candidate state on list) the match was, on the average, found after searching a fraction 0.46 of the entries in the data base. A histogram of this fraction is given in Figure 18[1]. Note how flat the distribution is. As we had to search many records to find the match (and so terminate step), it will turn out to be straightforward to find a concurrent algorithm as the search time (step 2) dominates the "sequential" steps 1 and 3 corresponding to generation of query and updating the data base. We should also note that the comparison of a candidate state with a pre-existing state is arranged hierarchically and that the comparison time varies from case to case. This inherent load imbalance due to the irregularity of the problem needs to be kept in mind for the concurrent algorithm.

[1] Note that most of the successful queries are generated with the data base nearly complete; i.e., initially most queries fail, the data base builds up, and then most queries succeed.

Appendix D

In Figure 19, we plot the inverse of the efficiency ε (sequential time divided by N times the time taken on the N node concurrent implementation) as a function of N in the range 1 to 32. Even for N=32 we find an efficiency of 60% in spite of the modest size of the local data base with a maximum of 28 entries. Clearly, the algorithm will perform better as the size of the data base increases. The approximate formula for the inverse of the efficiency is :

$$\frac{1}{\varepsilon} = \frac{N^* \text{concurrent time}}{\text{sequential time}} = \tag{D1}$$

$$= \frac{N\left(\frac{g^*M^*Q}{c_1^*N} + d^*Q + c_2^*b^*Q\ \log_2 N\right)}{\frac{g^*M^*Q}{c_1} + d^*Q}. \tag{D2}$$

Here we put c_1 equal 2 because in average only half of the data base is searched for query (see Figure 1, Table 1). For the constant c_2 we took 2/3 because nodes communicate only for failed queries. With these values of constants c_1 and c_2 equation (D2) takes form:

$$\frac{1}{\varepsilon} = \frac{1 + \frac{2d}{g^*M}N + \frac{4b}{3g^*M}N\log_2 N}{1 + \frac{2d}{g^*M}}, \tag{D3}$$

where

g – time spent on query per state,

d – time spent to produce query,

b – time to broadcast message,

Q – number of queries,

M – size of the data base.

The logarithmic dependence on N is expected as this is dependence of communication time for the broadcast message passing used in the algorithm.

Constants d and g can be calculated, using data included in the Table 1, from the following formulas :

$$g = \frac{\text{sequential time}}{\text{number of data base comparisons}} = 5.76ms \qquad \text{(D4)}$$

$$d = \frac{\text{sequential time*fraction of time spent generating queries}}{\text{number of queries}} = 51ms \qquad \text{(D5)}$$

Equation (D1) is compared with the results in Fig. 19. Values of the constants g and d are taken from Eqs. (D4) and (D5) and constant b, regarded as a free parameter, is fitted to be 1.41. The exact value of b is difficult to predict due to the asynchronous, independent operation of nodes. One would expect $b\log_2 N$ to be roughly the time taken for a broadcast message to traverse half the cube. This model would predict b to be 1 ms, which is in satisfactory agreement with the fitted value[2].

[2] The value of b could be reduced by about a factor of two using a full assembly language coding [15].

References

[1] K. G. Wilson, Phys. Rev. D14, 2455 (1974).

A. M. Polyakov, Phys. Lett. B59, 82 (1975).

F. Wegner, J. Math. Phys. 12, 2259 (1971).

[2] J. Kogut, L. Susskind, Phys. Rev. D11, 395 (1975).

[3] P.Hasenfratz, *Lattice Quantum Chromodynamics* , Published in Schladming School Proceedings (1983).

[4] A. Hasenfratz, P.Hasenfratz, Phys. Lett. 93B, 165 (1980).

[5] R. Dashen, D. Gross, Phys. Rev. D23, 2340 (1981).

[6] M. Creutz, Phys. Rev. Lett. 45, 313 (1980).

[7] M. Creutz, M. Moriarty, Phys. Rev. D26, 2166 (1982).

[8] K. Osterwalder, E. Seiler, Ann. Phys. (NY) 110, 440 (1978).

[9] E. P. Wigner, *Group Theory*, Academic Press, New York (1959);

see also

A. Edmonds, *Angular Momentum in Quantum Mechanics*, Princeton Univ. Press, Princeton, New Jersey.

[10] E. Mathieu, *Memoire sur le movement vibratoire d'une membrane de form elliptique*, J. Math. Pures Appl. 13 (1868) 137.

see also

N. W. McLachlan, *Theory and Application of Mathieu Functions*, Clarendon Press, Oxford, England, (1947).

[11] M. Creutz, Phys. Rev. D21, 2308 (1980).

[12] B. Berg, A. Billoire, C. Rebbi, Ann. Phys. 142 (1982) 185.

[13] W. Furmanski, A,Kolawa, *Yang-Mills Vacuum - An Attempt of Lattice Calculus*, CALT–68–1330 (1986).

[14] G. C. Fox, A. Kolawa, *Concurrent Searching of a Data Base - An Application of the Hypercube to Symbolic Quantum Chromodynamics*, CALT–68–1296 (1985).

[15] M. Johnson, *An Interrupt Driven Communications System*, January 1985 (unpublished)

[16] M. Gell–Mann, F. Low, Phys. Rev. 95, 1300 (1954).

Petermann and Stueckelberg, Helv. Phys. Acta 26, 499 (1953).

H. D. Politzer, Phys. Rev. Lett. 30, 1346 (1973).

D. Gross, F. Wilczek, Phys. Rev. Lett. 30, 1343 (1973).

D. Gross, F. Wilczek, Phys. Rev. D8, 3633 (1973).

W. E. Caswell, Phys. Rev. Lett. 33, 244 (1974).

D. R. T. Jones, Nucl. Phys. B75, 531 (1974).

[17] N. Metropolis, et. al., J. Chem. Phys. 21, 1087 (1953).

5, *Monte Carlo Methods in Statistical Physics*, edited by K. Binder, Springer–Verlag,New York, (1979).

[18] R. Balian, J. M. Drouffe, C. Itzykson, Phys. Rev. D11, 2104 (1975)

E. Brezin, J. M. Drouffe, Nucl. Phys. B200, 93 (1982).

V. Alessandrini, V. Hakim, A. Krzywicki, Nucl. Phys. B215, 109 (1983).

V. Alessandrini, Phys. Lett. 117B, 423 (1982).

V. Alessandrini, P. Boucaud, Nucl. Phys. B235, 599 (1984).

J. Greensite, B. Lautrup, Phys. Lstt. 104B, 41 (1981).

H. Flyvbjerg, B. Lautrup, J. B. Zuber, Phys. Lett. 110B, 279 (1982).

B. Lautrup, W. Ruhl, Z. Phys. C23, 49 (1984).

V. F. Muller, W. Ruhl, Nucl. Phys. B210, 289, (1982).

S. Elitzur, Phys. Rev. D12, 3978 (1975).

[19] J. B. Kogut, R. B. Pearson, J. Shigemitsu, Phys. Rev. Lett. 43, 484 (1979).

J. B. Kogut, J. Shigemitsu, Phys. Rev. Lett. 45, 410 (1980).

J. B. Kogut, R. B. Pearson, J. Shigemitsu, Phys. Lett. 98B, 63 (1981).

G. Munster, Phys. Lett. 95B, 59 (1980).

G. Munster, Nucl. Phys. B190, 439 (1981).

G. Munster, P. Weisz, Phys. Lett. 96B, 119 (1980).

G. Munster, Nucl. Phys. B256 (1985).

G. Munster, Phys. Lett. 121B (1983).

K. Seo, Nucl. Phys. B209, 200 (1982).

J. Smit, Nucl. Phys. B206, 309 (1982).

A. Hasenfratz, E. Hasenfratz, P. Hasenfratz, Nucl. Phys. B181, 353 (1981).

C. Itzykson, M. Peskin, J. B. Zuber, Phys. Lett. B95, 259 (1980).

M. Luscher, G, Munster, P. Weisz, Nucl. Phys. B180, 1 (1980).

[20] We give here references to the microcanonical method which originated from the high temperature Hamiltonian expansion.

J. Polonyi, H. W. Wyld, Phys. Rev. Lett. 51, 2257 (1983).

J. Polonyi, H. W. Wyld, J. Kogut, J. Shigemitsu, D. K. Sinclair, Phys. Rev. Lett. 53, 644 (1984).

J. Kogut, J. Polonyi, H. W. Wyld, D. K. Sinclair, ILL–(TH)–85–6, (1985)preprint.

Figure captions

Fig. 1 Monte Carlo calculations of string tension for $SU(2)$ gauge theory.

Fig. 2 Monte Carlo calculations of string tension for $SU(3)$ gauge theory.

Fig. 3 Correlation length as a function of β for $SU(2)$ gauge theory.

Fig. 4a 3r vertex–our choice for the parameterization of the SU(2) rank 6 invariant tensor.

Fig. 4b Triangle inequality for rrr and lrl vertices.

Fig. 5a Fragment of the triangulised surface, illustrating geometrically the triangle inequality constraints.

Fig. 5b Plaquette with all attached pipes – planar picture (dotted lines indicate correct directions).

Fig. 6 Derivation of the deformation amplitudes – step 1: reduction on links.

Fig. 7 Derivation of the deformation amplitudes – step 2: reduction in vertices.

Fig. 8 Derivation of the deformation amplitudes – step 3: final result.

Fig. 9 Reduction of the one–loop vertex diagram: w = Wigner symbol.

Fig. 10 A typical solution to the Equation 3.15.

A straight line presents LHS of Equation 3.15

Distance between a and b is the mass gap

Continuous curves present the RHS of equation 3.15

Fig. 11 States from the second generation.

Fig. 12aExamples of the loop zero modes (ambiguities in the loop representation).

Fig. 12b Examples of typical transition amplitudes for small loops.

Fig. 12c Decay process $\sigma \to \tau_1, \tau_2$, contributing to the vertex $J_{\sigma,\tau_1\tau_2}$.

Fig. 13 Diagrammatical conventions for the connected vertices.

Fig. 14a Schrodinger equations.

Fig. 14b and 14c Building Mathieu fraction by solving the equations for correlations and inserting the result to the loop equations.

Fig. 15 Loops up to $\sigma_0 = 3$.

Fig. 16 Mass of 0^{++} glueball in $SU(2)$ gauge theory as a function of β.

Lines 1 and the dashed area presents Monte–Carlo results together with statistical errors

Line 2 is the high temperature expansion

Lines 3–5 present different approximations in calculations for the glueball mass,

Line 3 contains only loops up to the second generation,

Line 4 loops up to the third generation

Line 5 loops up to the third generation plus disconnected two plaquette states

Fig. 17 Values of vacuum wave functions as functions of β.

Fig. 18 Histogram of the number of successful queries vs. the number of comparisons for sequential implementation.

Fig. 19 Plot of the inverse of efficiency vs. $\log_2$ of the number of nodes. The solid line is the plot of formula D3 and crosses are the measured values.

Fig. 20 Action of the operator V_p on a physical state

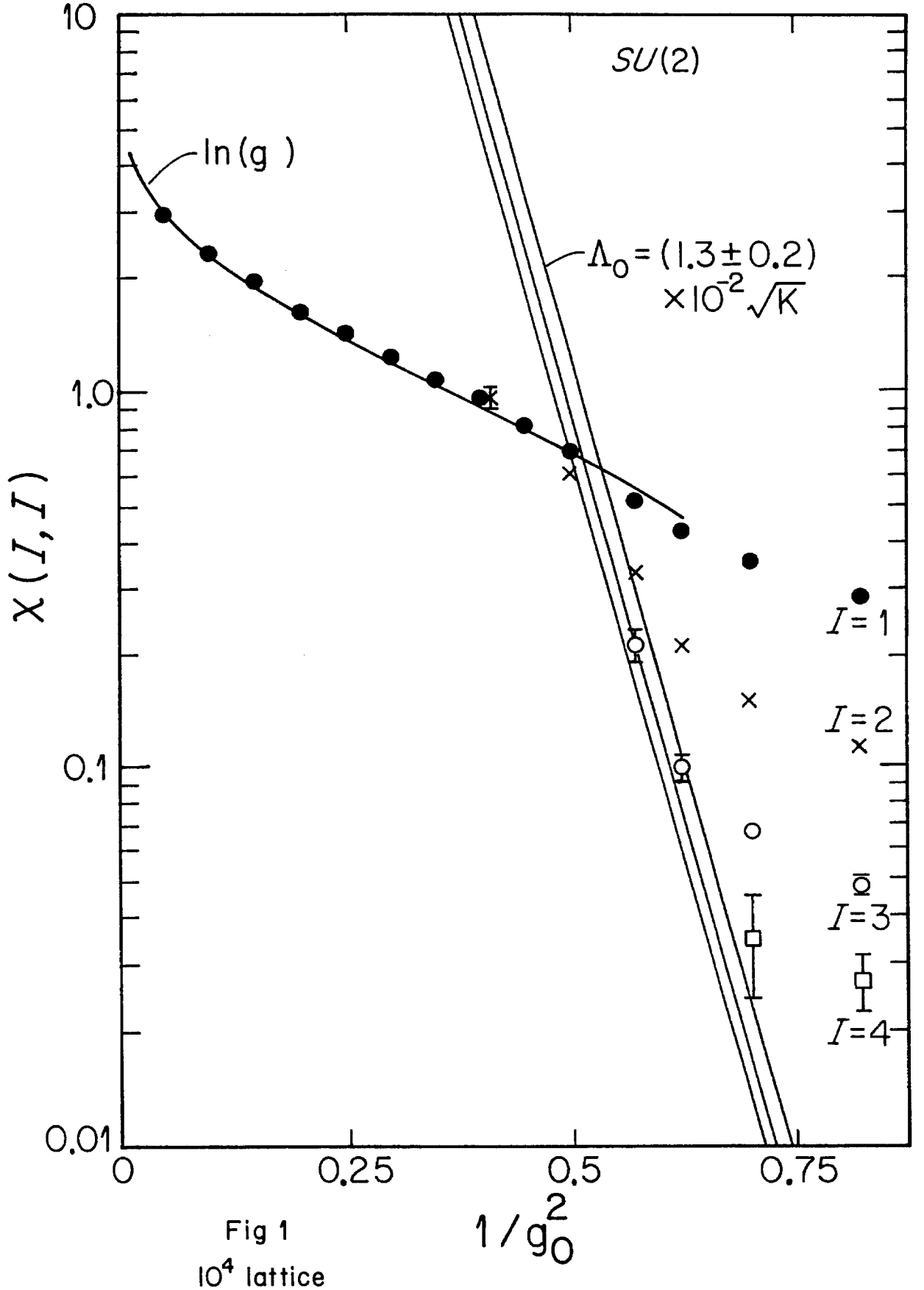

Fig 1

10^4 lattice

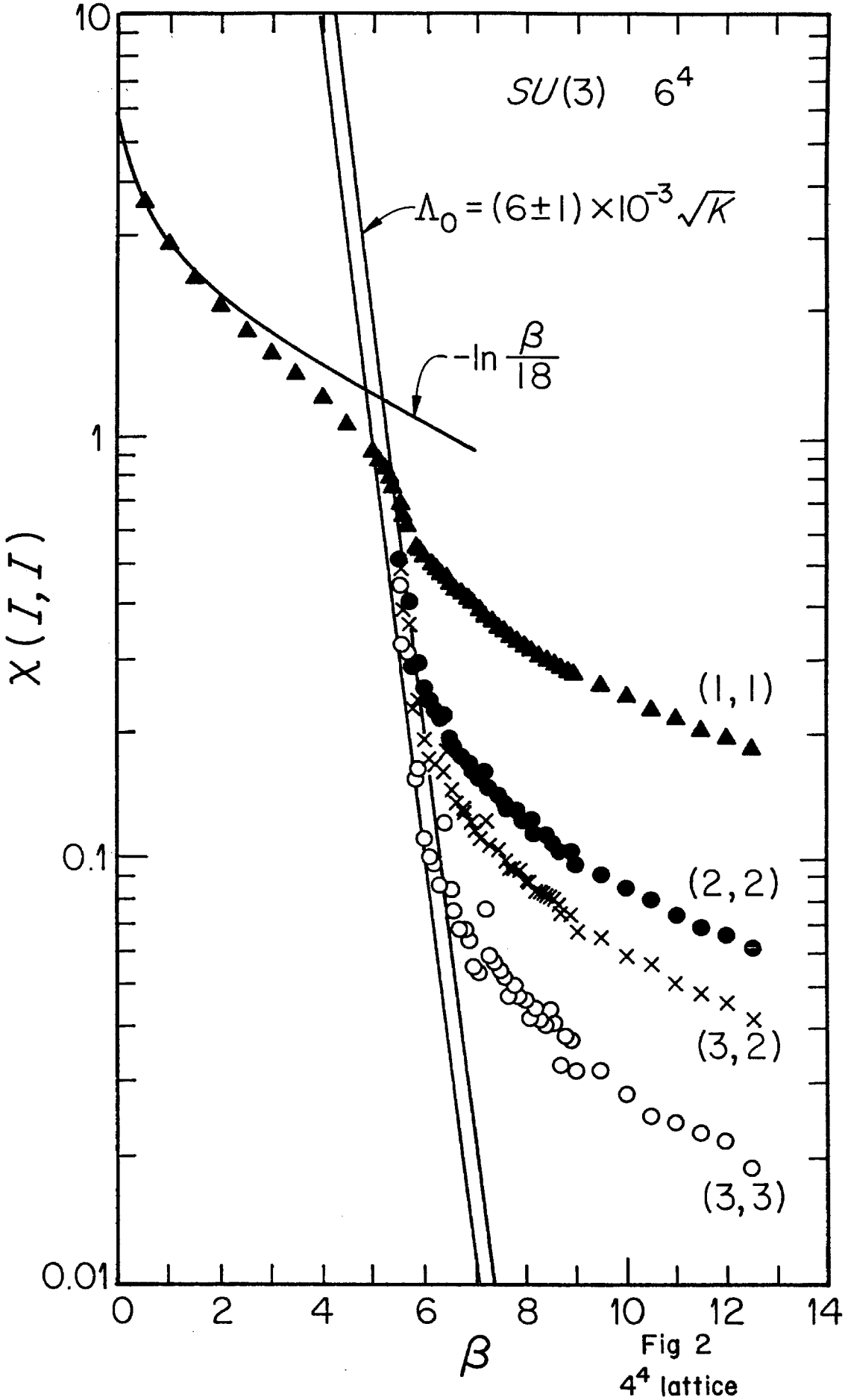

Fig 2
4^4 lattice

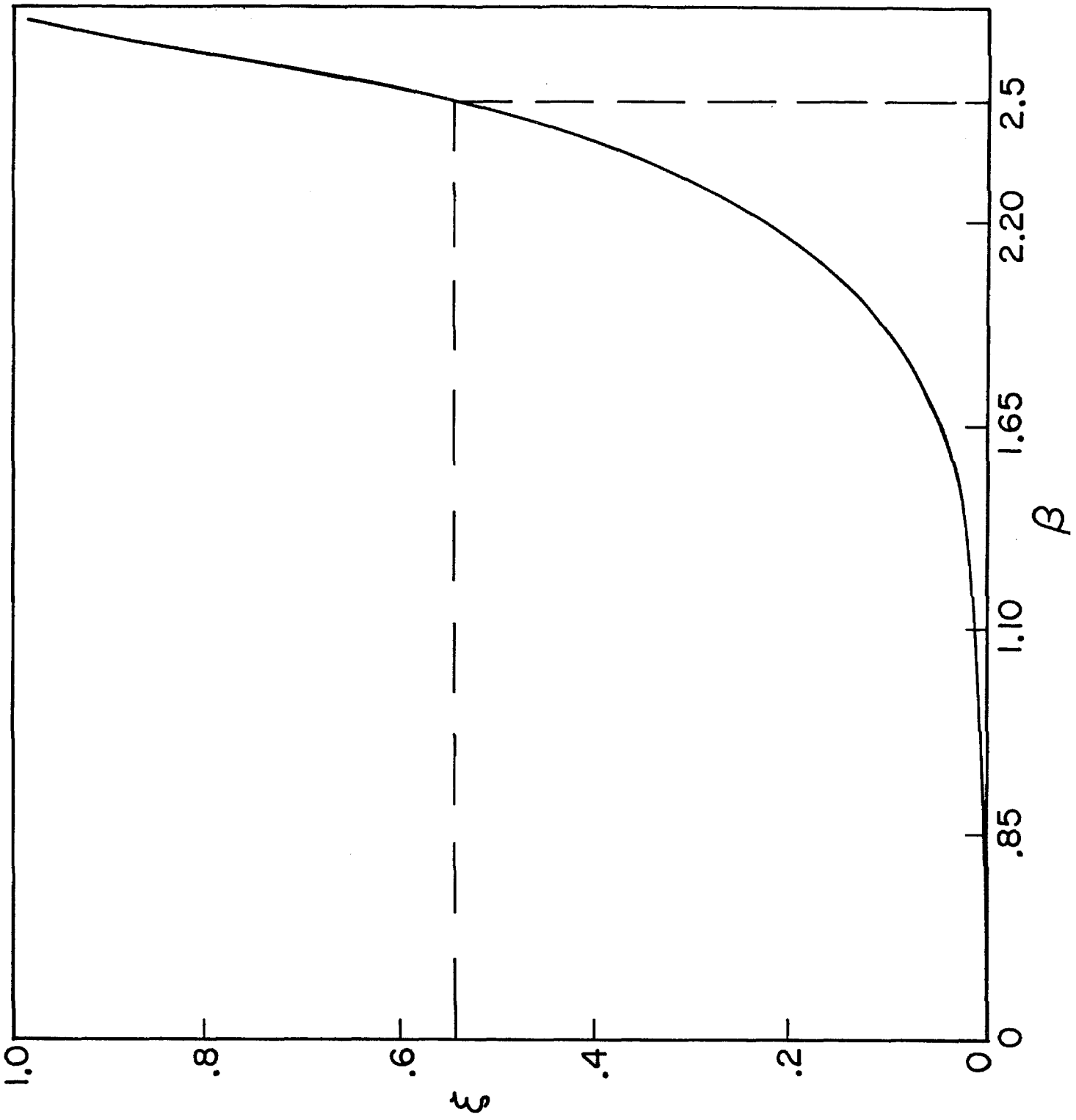

Fig. 3

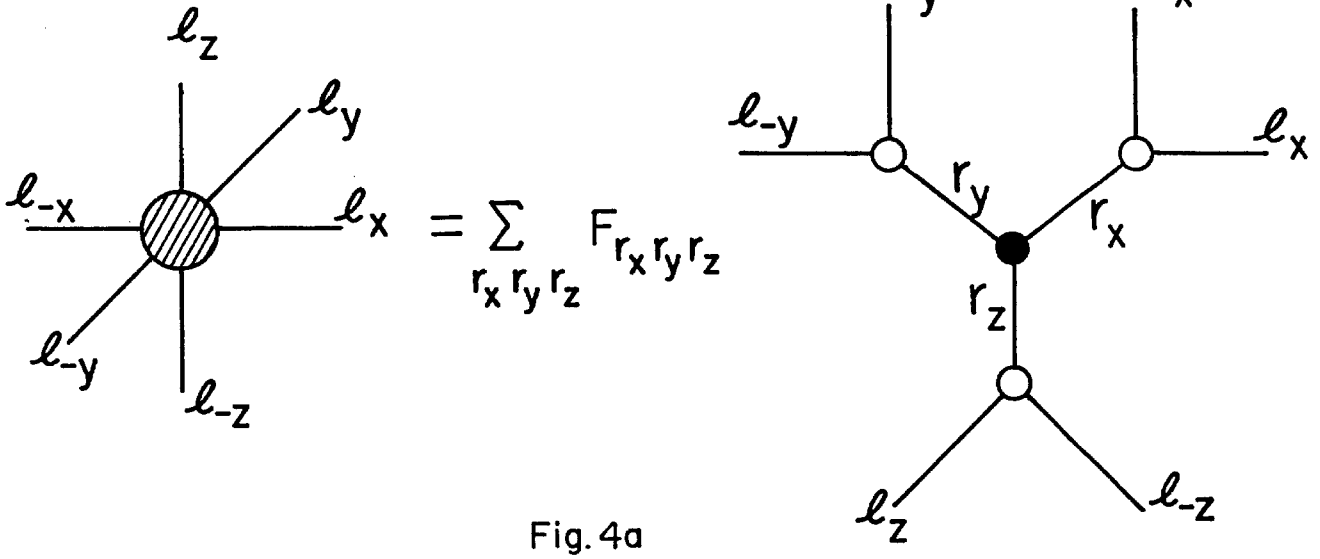
ℓ_z
ℓ_y
ℓ_{-x}
ℓ_x
ℓ_{-y}
ℓ_{-z}
$= \sum_{r_x r_y r_z} F_{r_x r_y r_z}$
ℓ_y
ℓ_{-x}
ℓ_{-y}
ℓ_x
r_y
r_x
r_z
ℓ_z
ℓ_{-z}

Fig. 4a

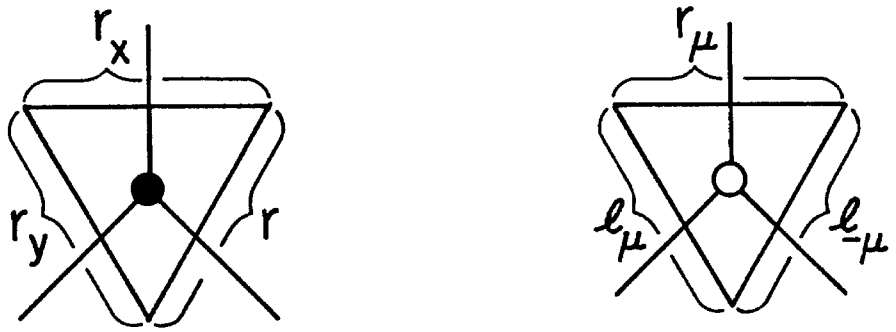
r_x
r_y
r
r_μ
ℓ_μ
$\ell_{-\mu}$

Fig. 4b

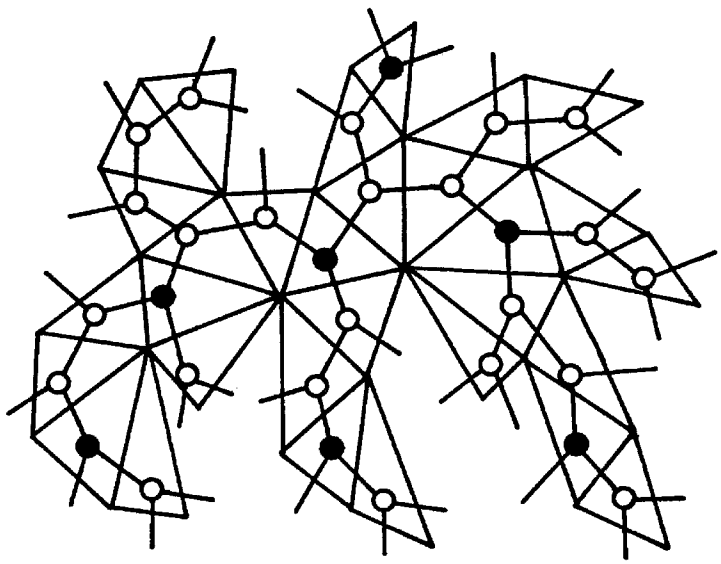

Fig. 5a

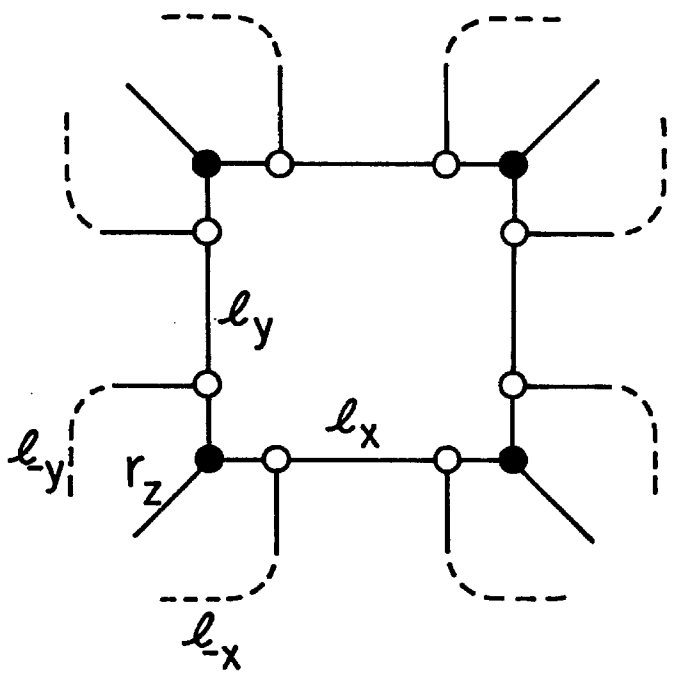

Fig. 5b

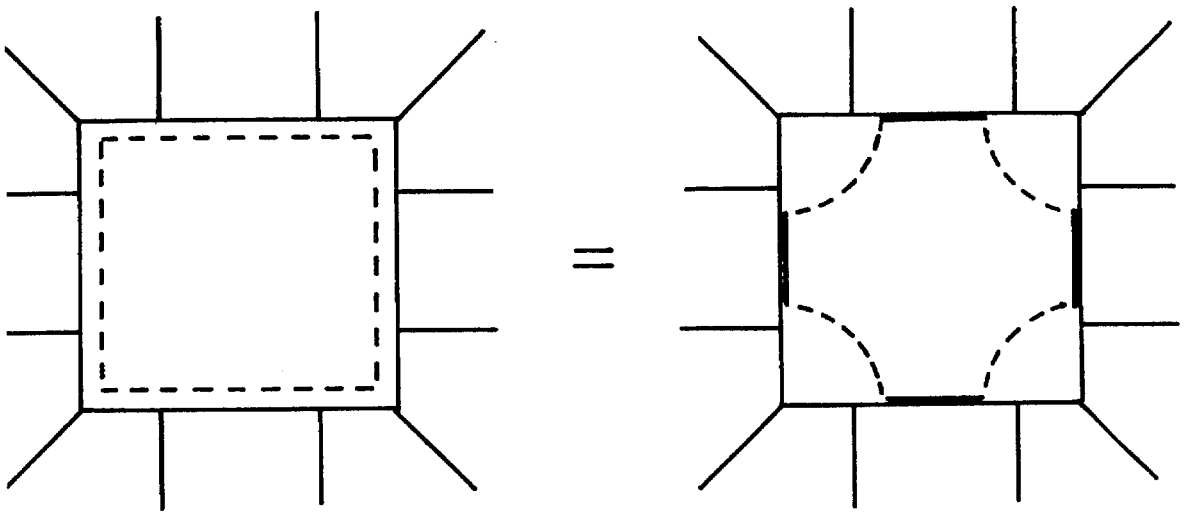

Fig. 6

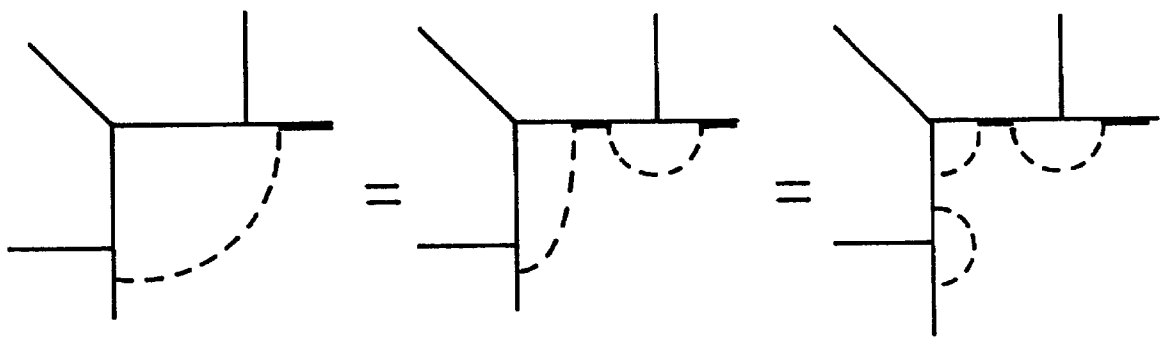

Fig. 7

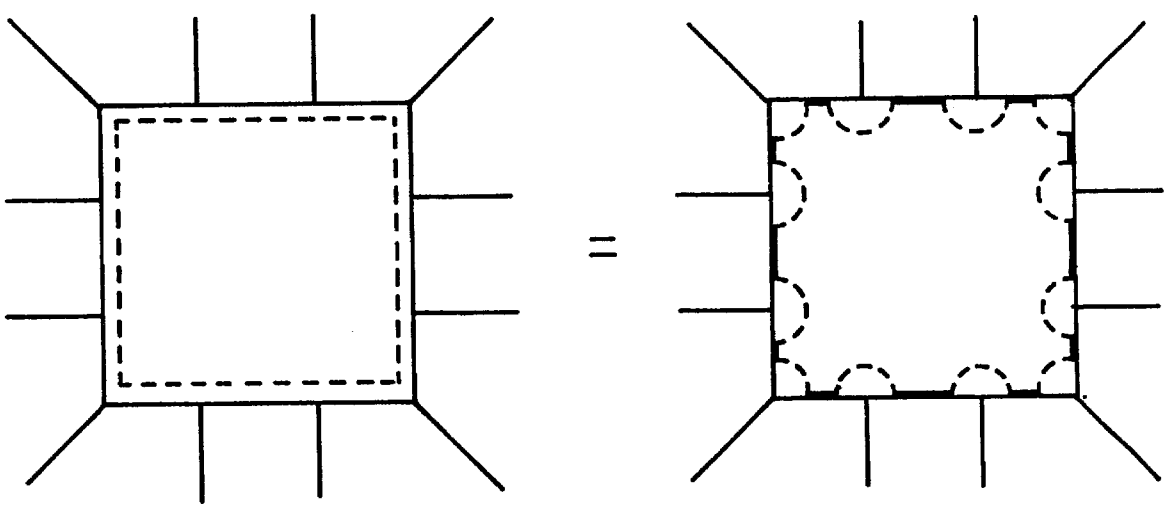

Fig. 8

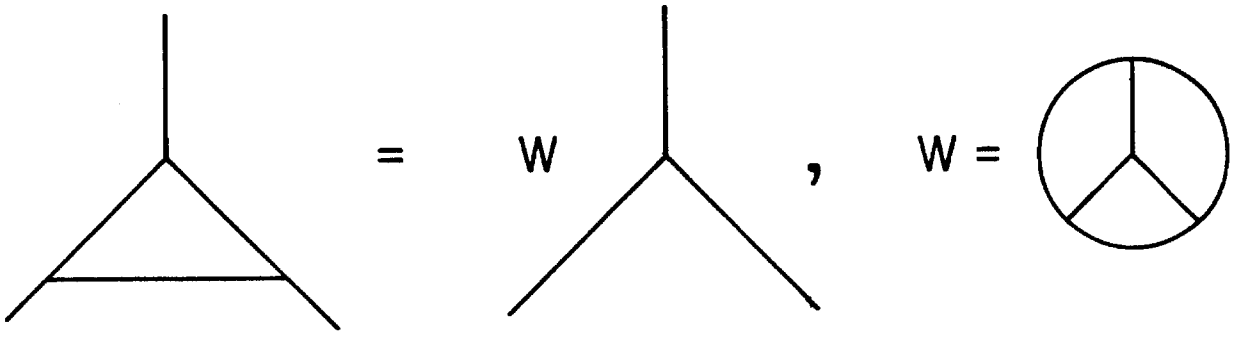

Fig. 9

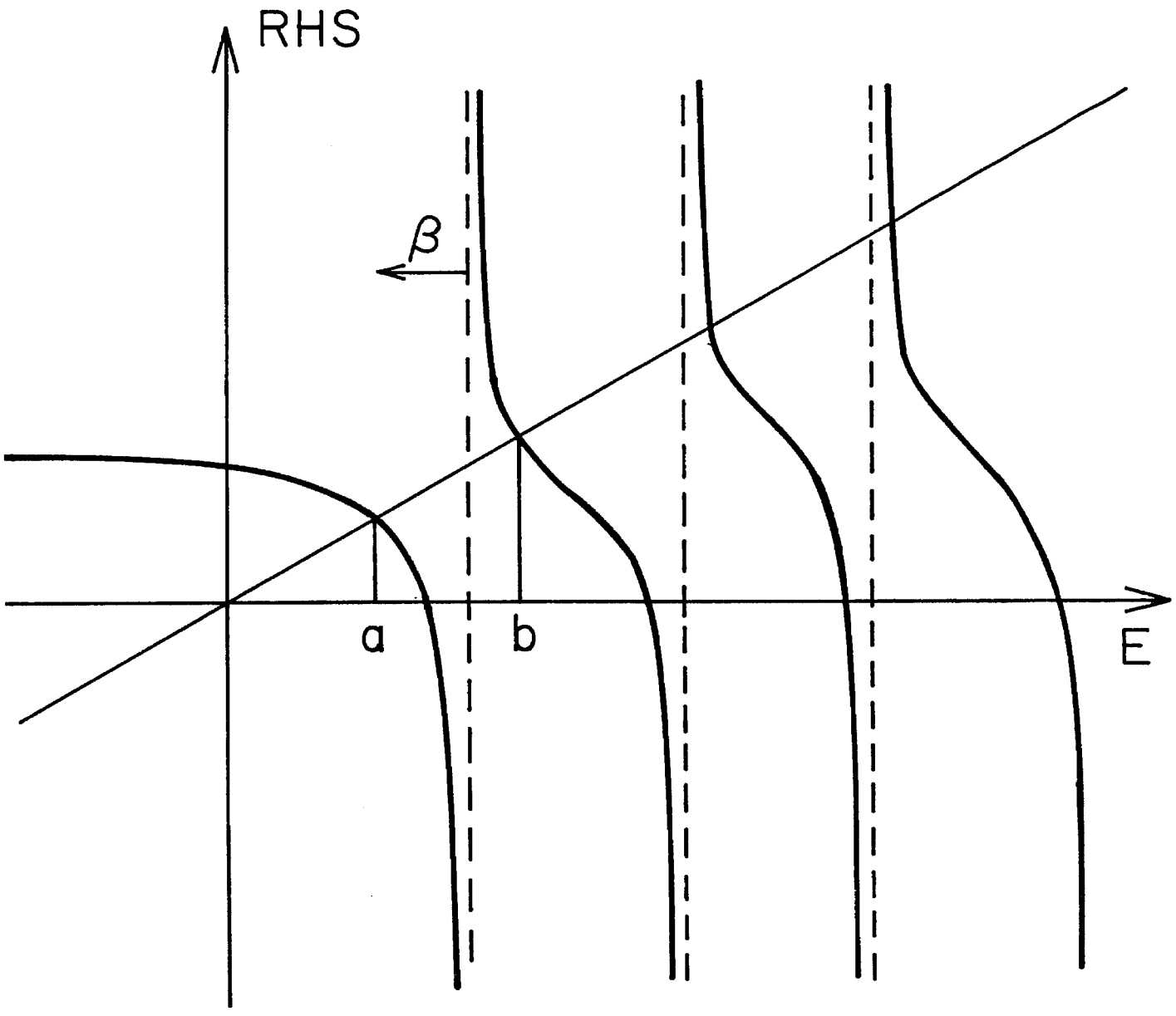

Fig. 10

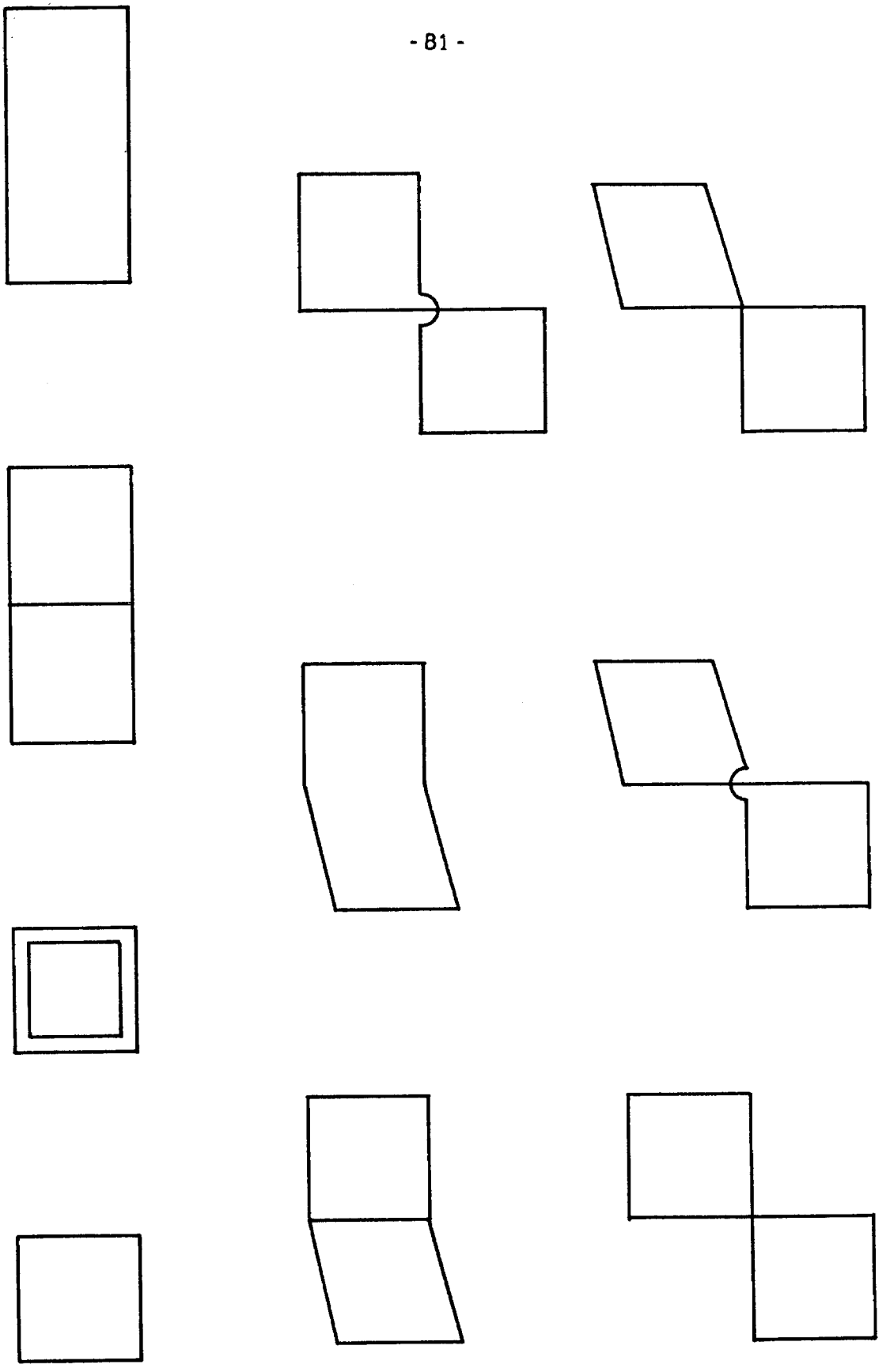

Fig. 11

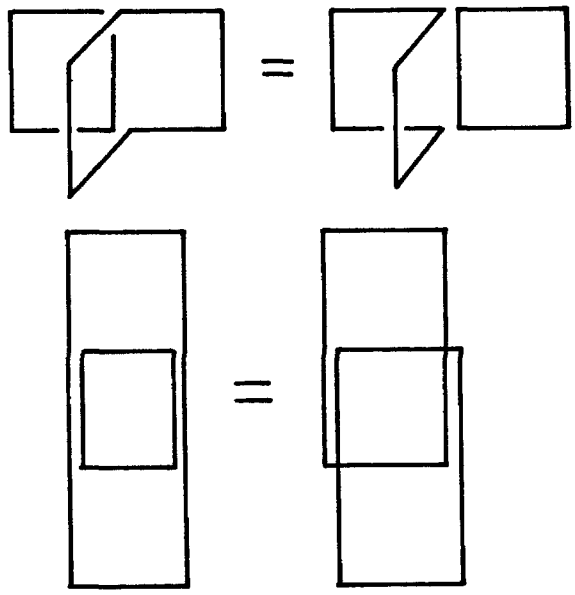

Fig. 12a

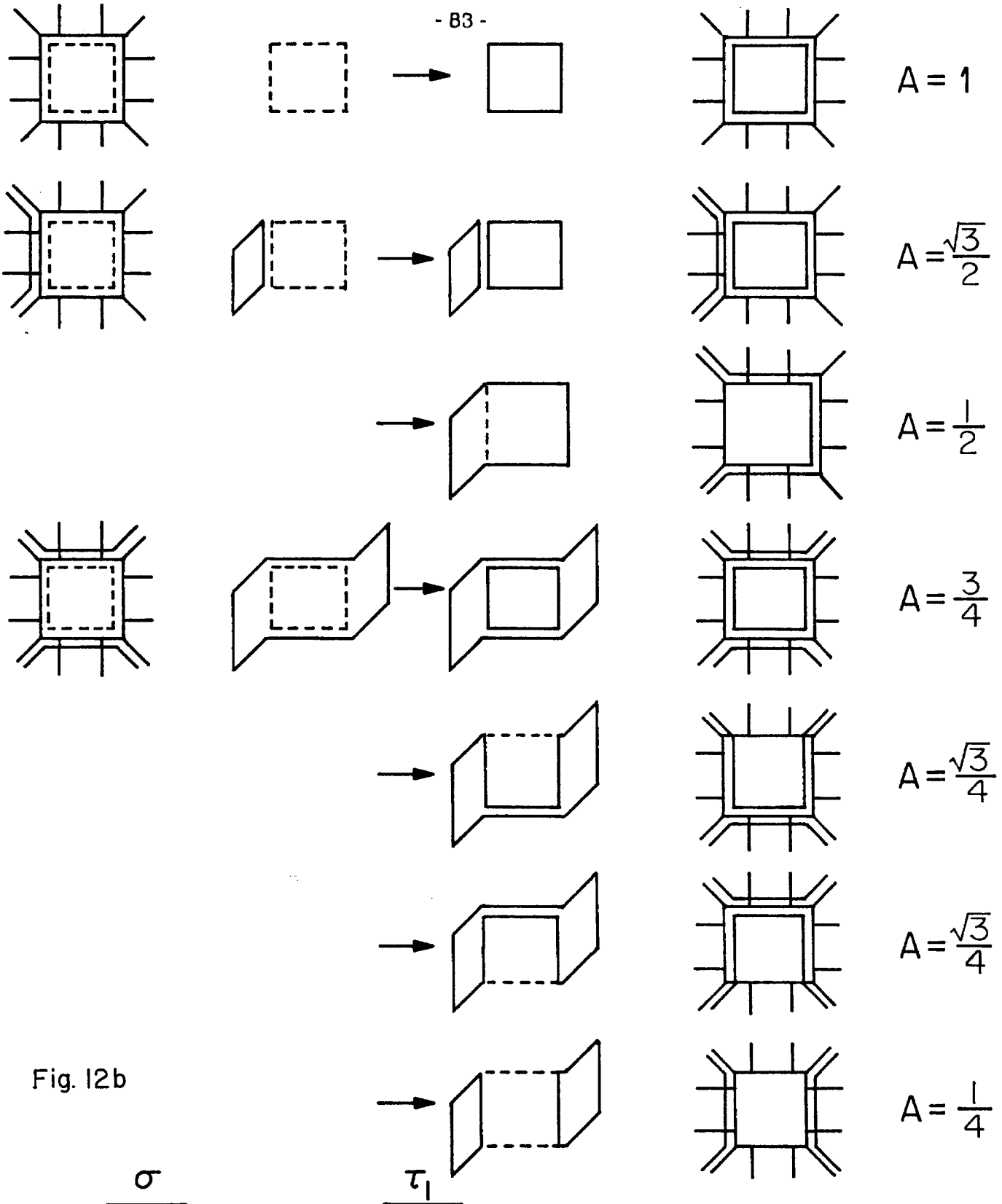

Fig. 12b

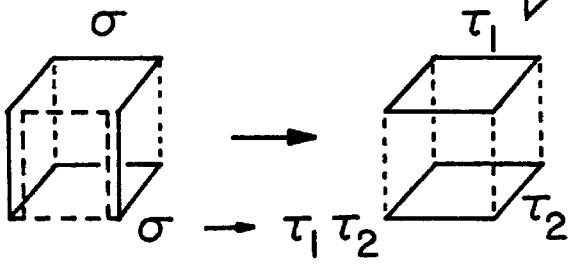

Fig 12c

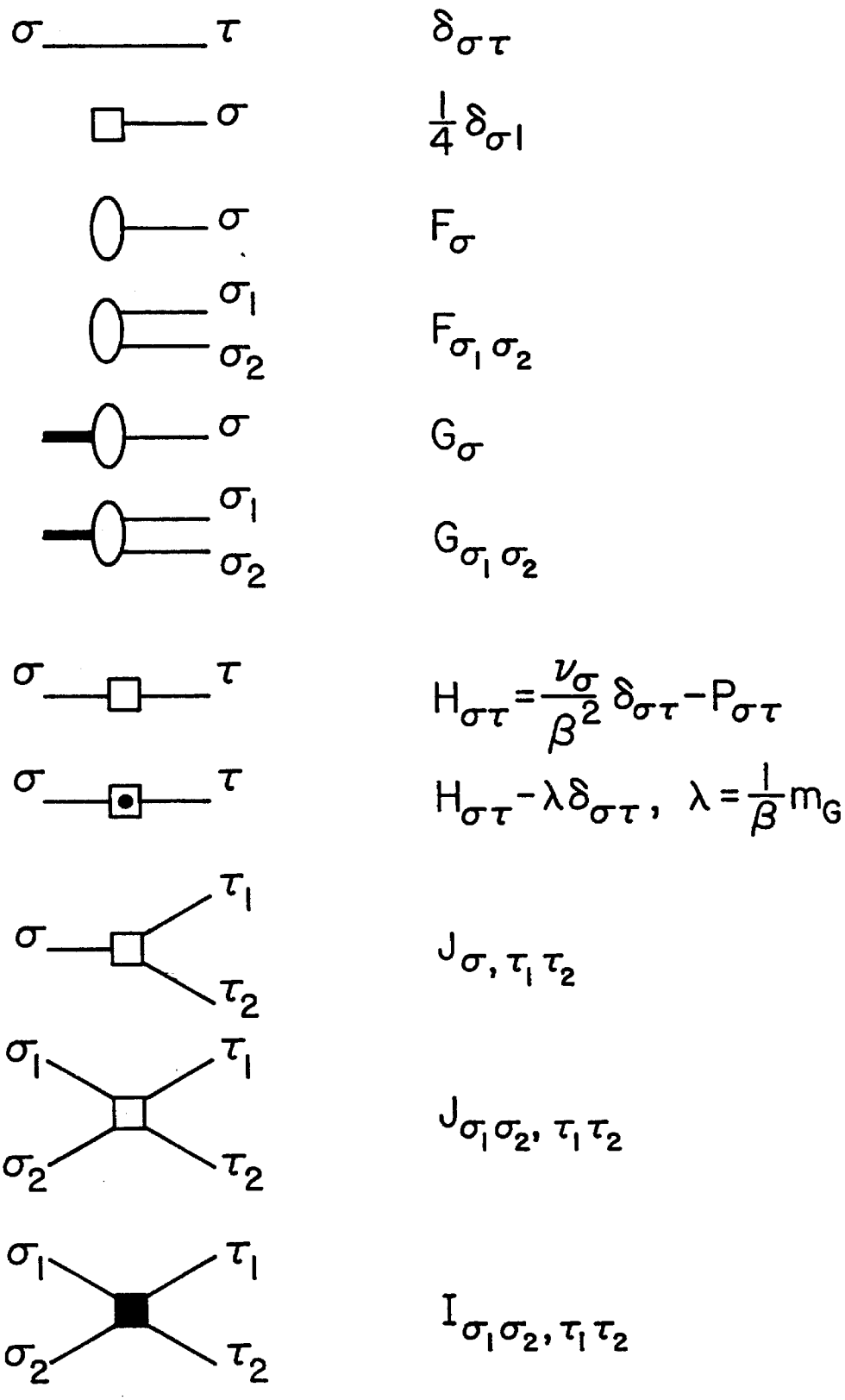
σ τ
$\delta_{\sigma\tau}$
σ
$\frac{1}{4}\delta_{\sigma 1}$
σ
F_σ
σ1
σ2
$F_{\sigma_1\sigma_2}$
σ
G_σ
σ1
σ2
$G_{\sigma_1\sigma_2}$
σ τ
$H_{\sigma\tau}=\frac{\nu_\sigma}{\beta^2}\delta_{\sigma\tau}-P_{\sigma\tau}$
σ τ
$H_{\sigma\tau}-\lambda\delta_{\sigma\tau},\ \lambda=\frac{1}{\beta}m_G$
σ
τ1
τ2
$J_{\sigma,\tau_1\tau_2}$
σ1
σ2
τ1
τ2
$J_{\sigma_1\sigma_2,\tau_1\tau_2}$
σ1
σ2
τ1
τ2
$I_{\sigma_1\sigma_2,\tau_1\tau_2}$

Fig. 13

VACUUM ENERGY

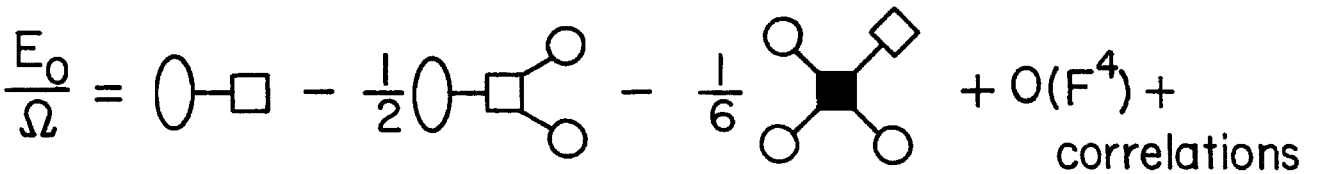

VACUUM EQUATIONS

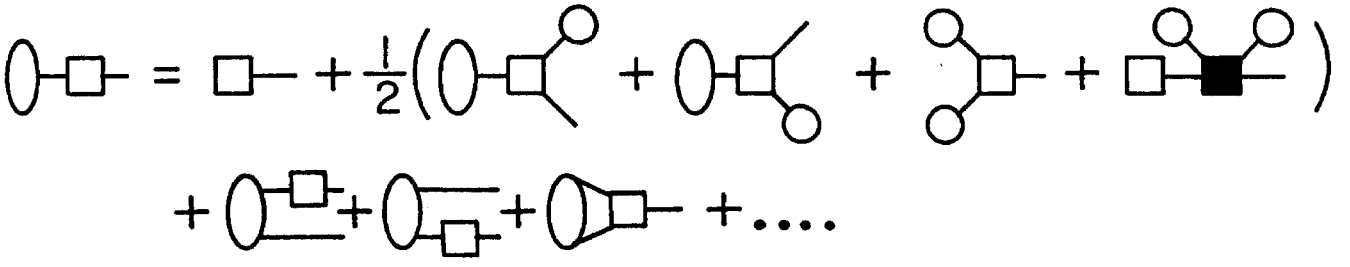

GLUEBALL EQUATIONS

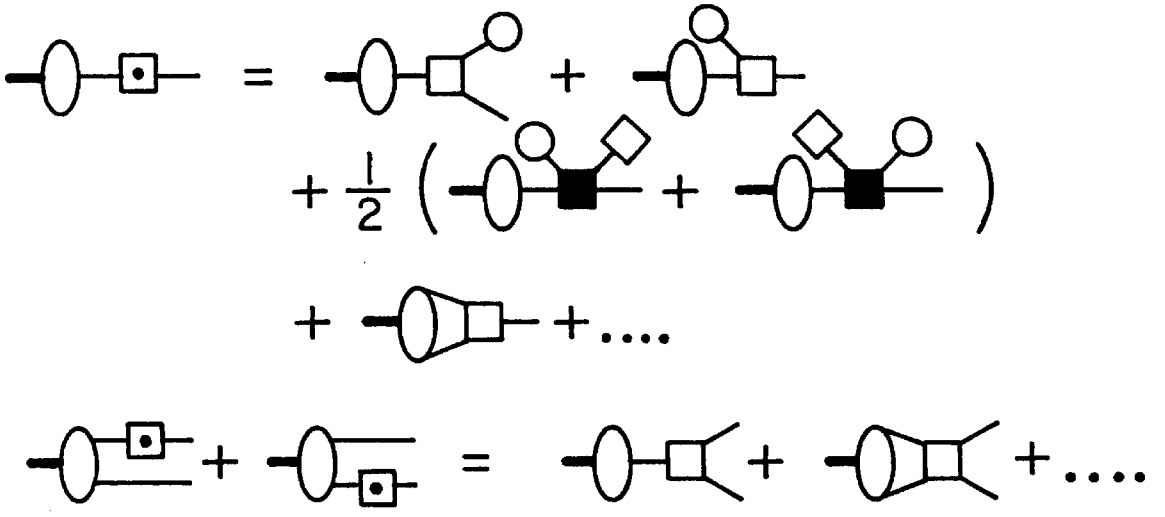

Fig. 14a

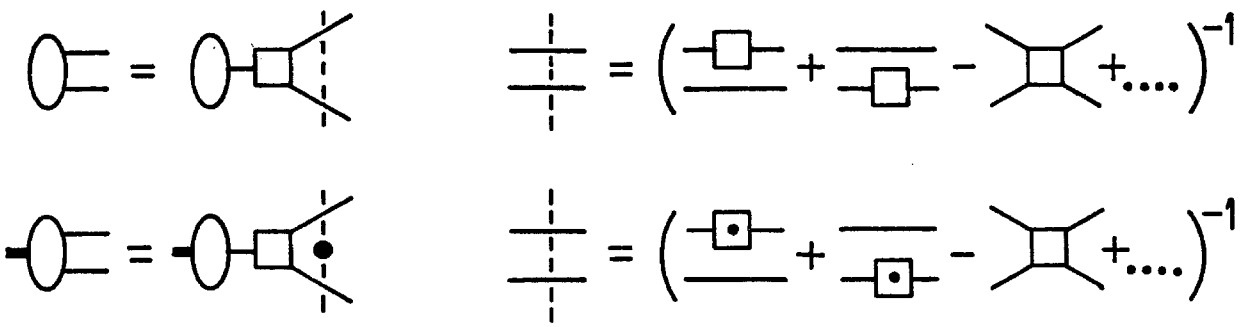

Fig. 14b

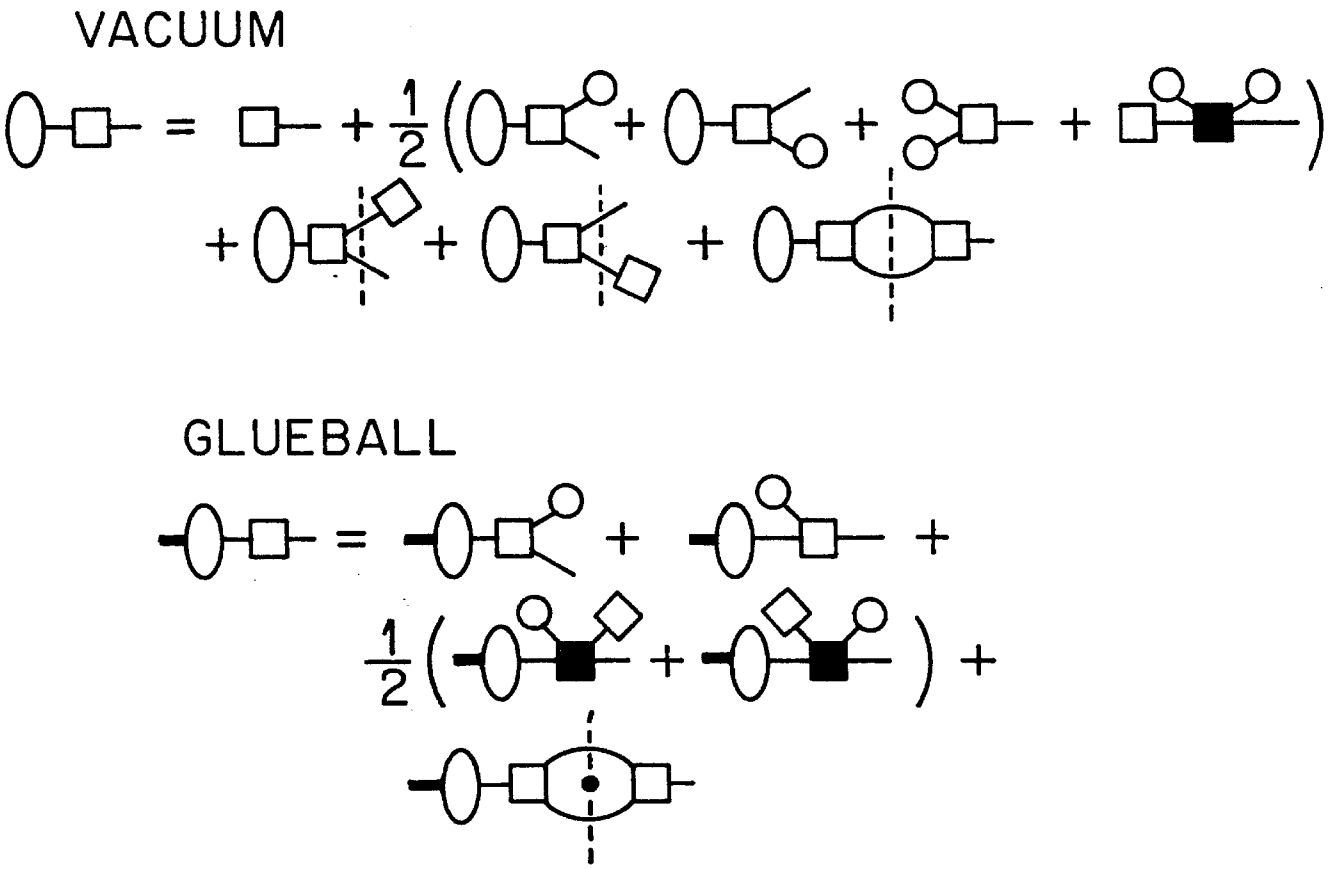

Fig. 14c

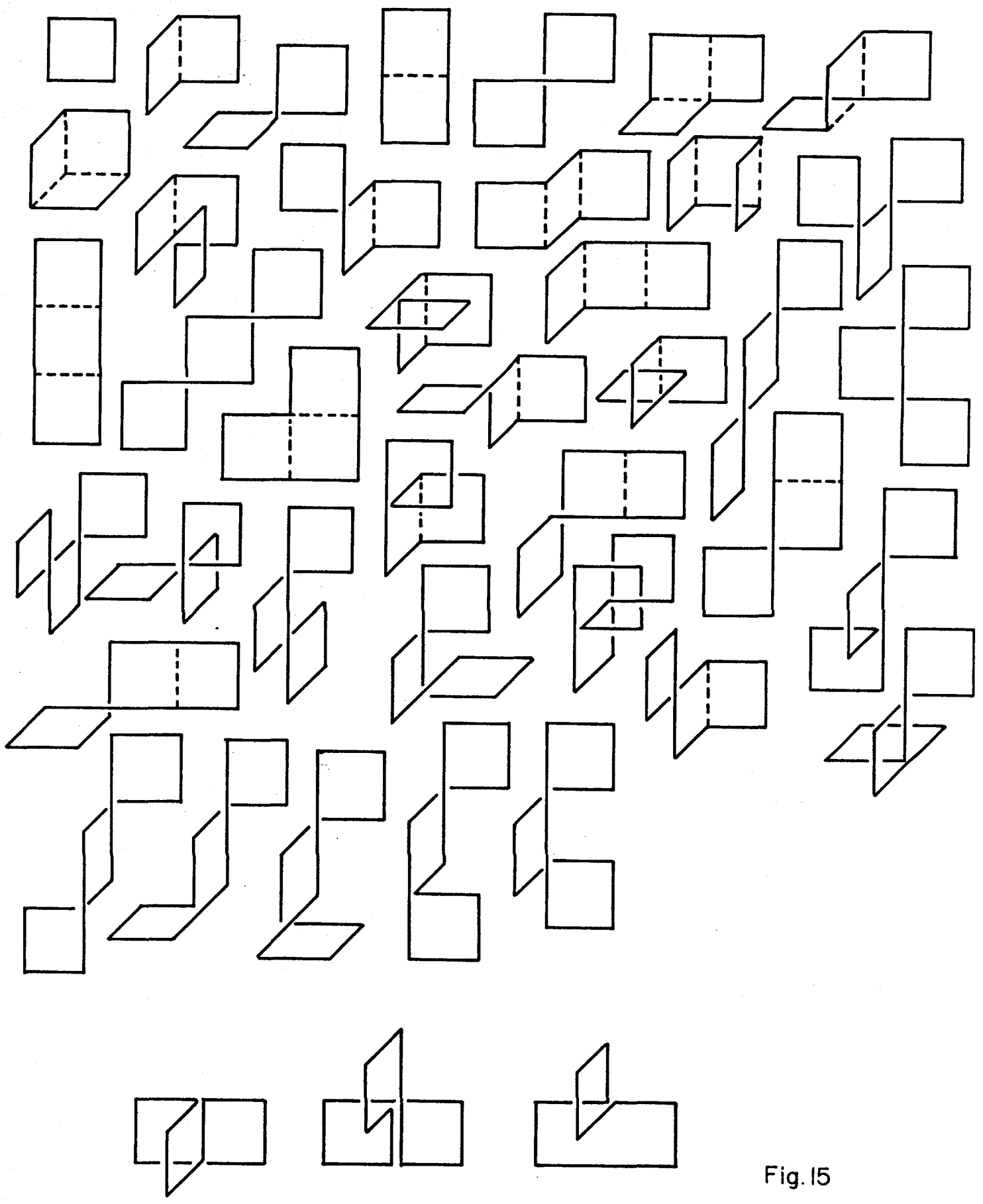

Fig. 15

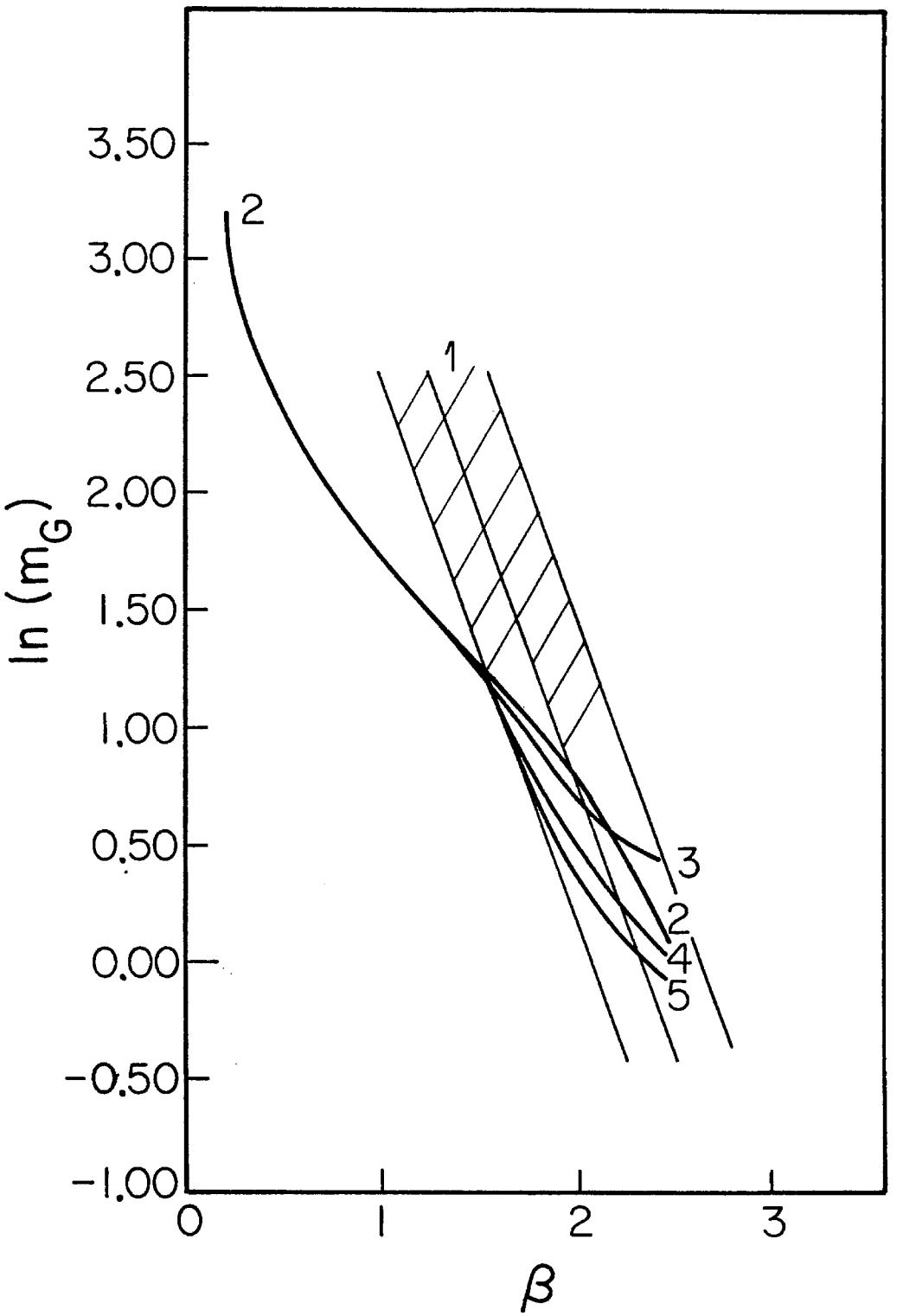

Fig.16

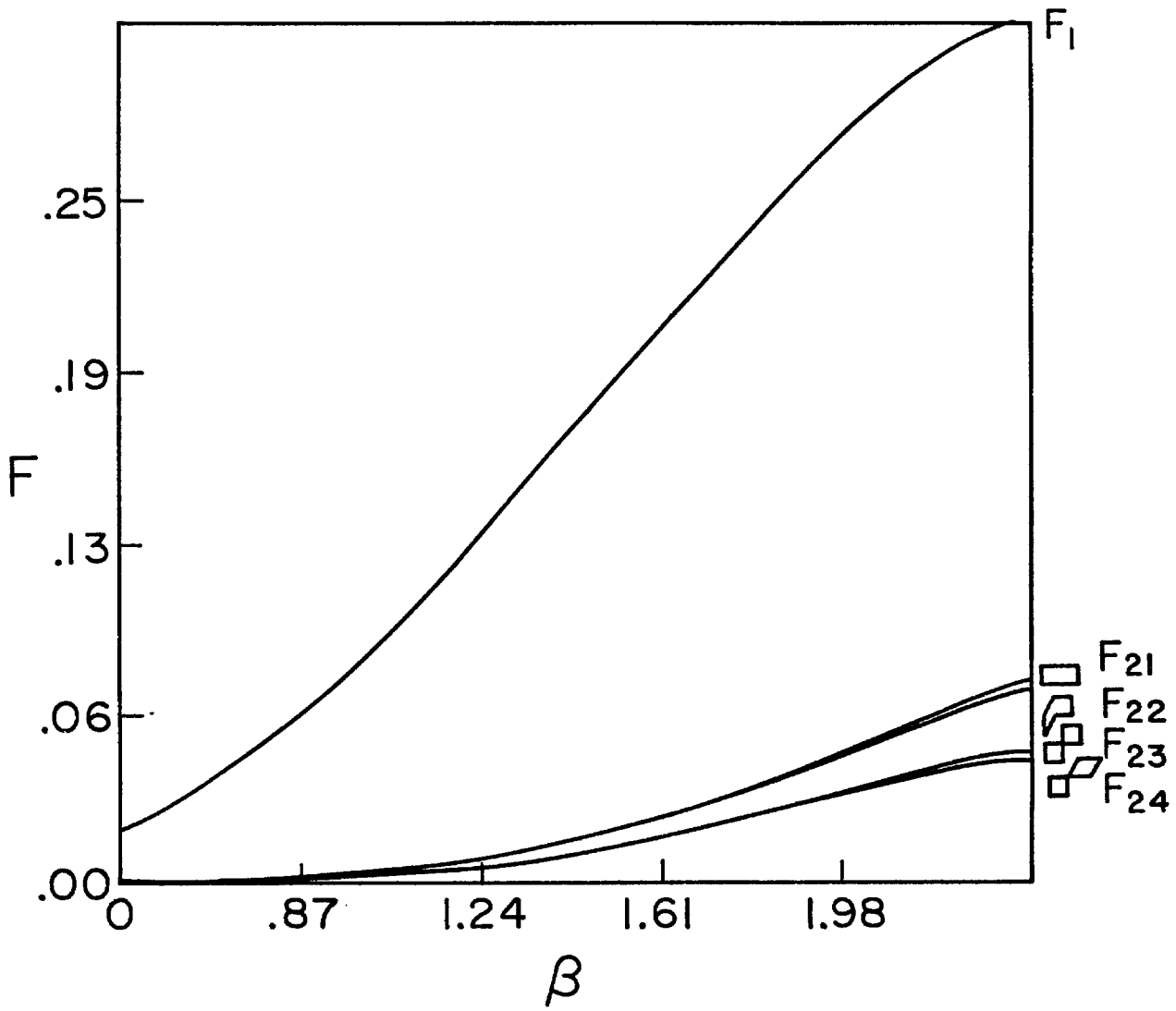

FIG. 17

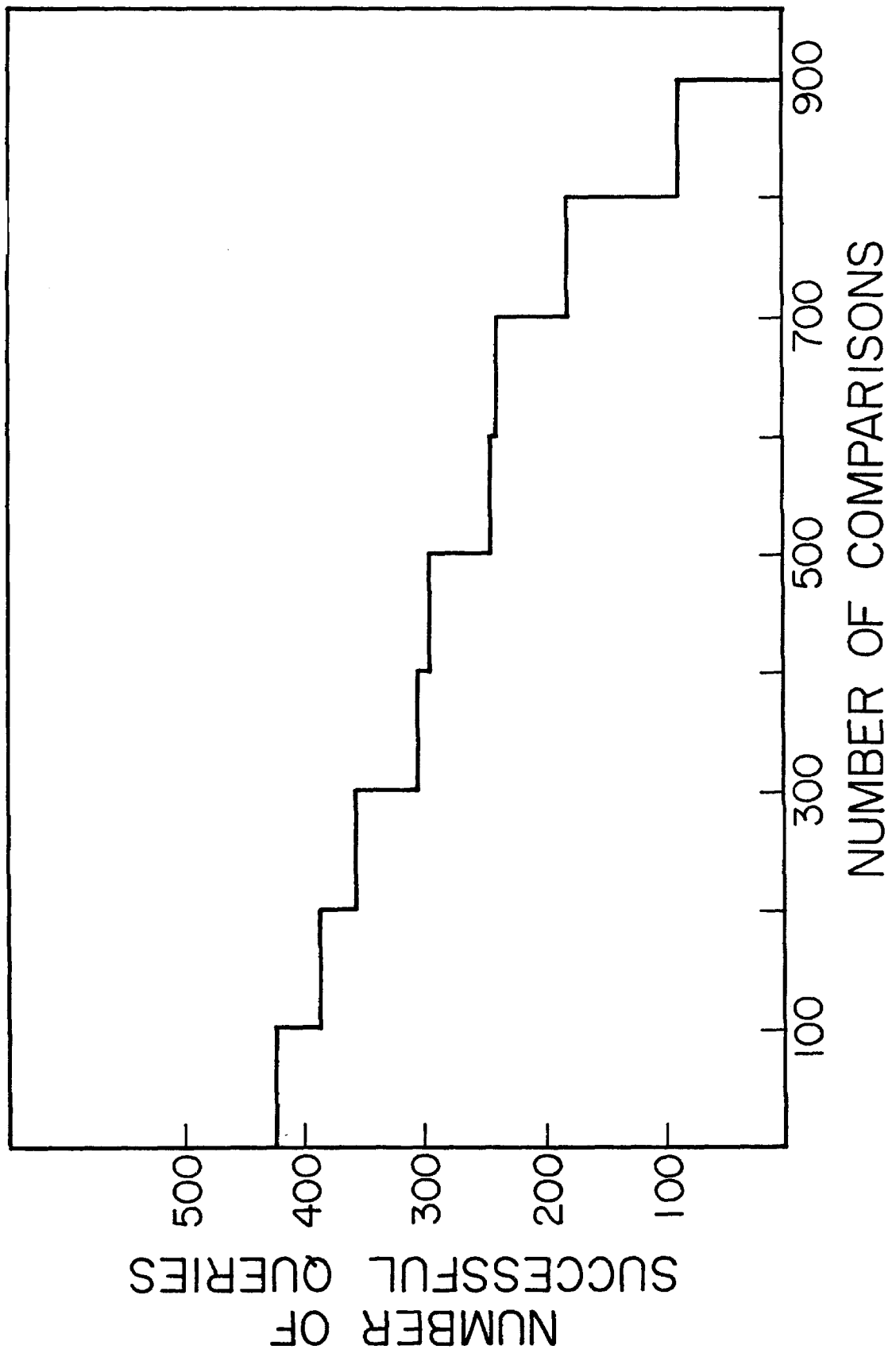
NUMBER OF SUCCESSFUL QUERIES
500
400
300
200
100
NUMBER OF COMPARISONS
100
300
500
700
900

Fig. 18

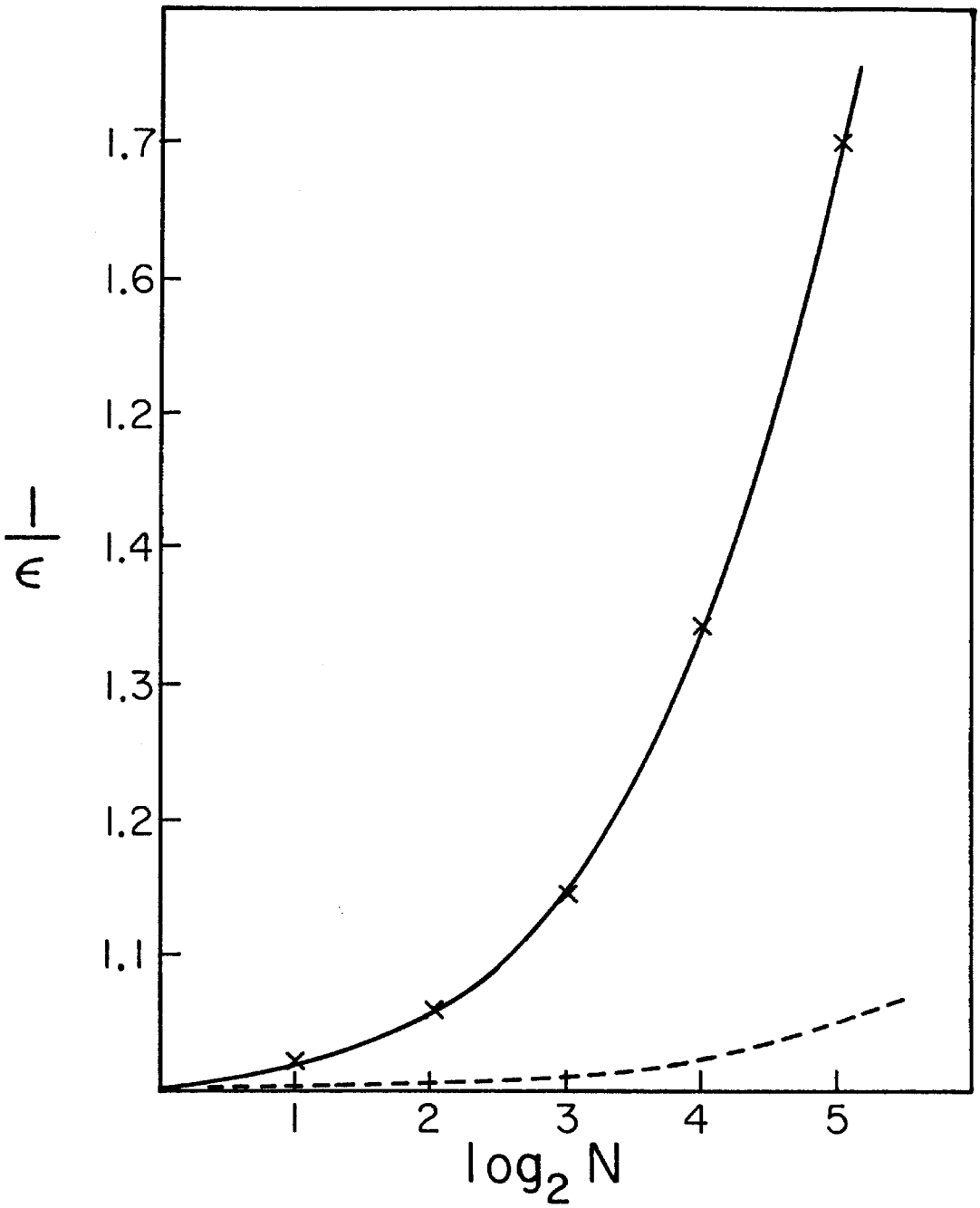

Fig. 19

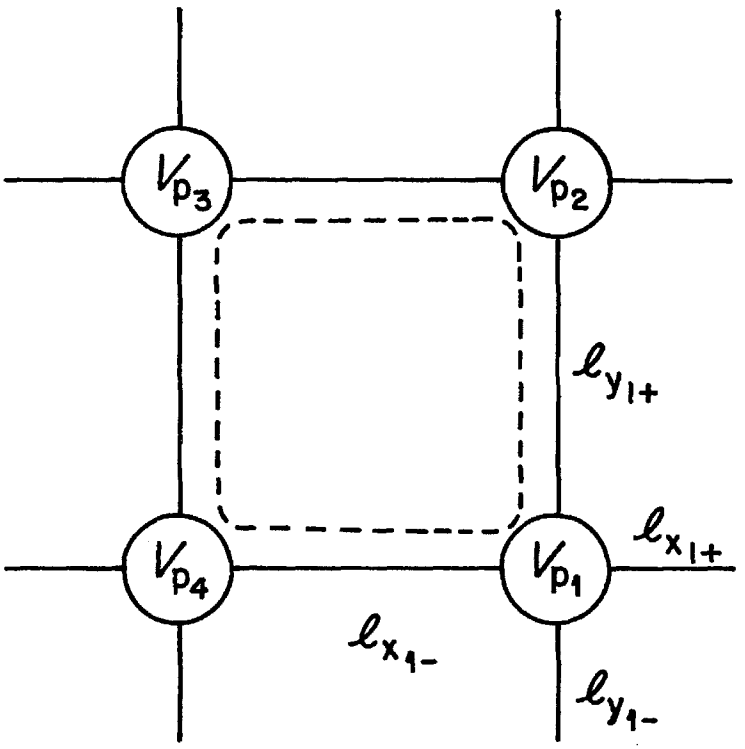

Fig. 20